Impacts of Global Warming on West African Monsoon rainfall: Downscaling by Pseudo Global Warming Method

Imoleayo E. Gbode[1,3,4], Kehinde O. Ogunjobi[2,3], Jimy Dudhia[3], Vincent O. Ajayi[4] and Changhai Liu[5]*

[1]West African Science Service Center on Climate Change and Adapted Land Use (WASCAL), Federal University of Technology Akure, Ondo State, Nigeria
[2]WASCAL Competence Center, Avenue Mouammar Kadhafi, Ouagadougou. Burkina Faso.
[3]Mesoscale and Microscale Meteorology Laboratory, National Center for Atmospheric Research, Boulder, CO, USA
[4]Department of Meteorology and Climate Science, Federal University of Technology Akure, Ondo State, Nigeria
[5]Research Applications Laboratory, National Center for Atmospheric Research, Boulder, CO, USA

*__Corresponding author:__ Imoleayo E. Gbode
__Email:__ iegbode@futa.edu.ng

Abstract

A set of numerical experiments was conducted in order to investigate the impacts of global warming on West African monsoon rainfall for selected five years. The experiments varied different cumulus, microphysics and planetary boundary layer parameterization schemes. Rainfall characteristics over three climatic zones, Guinea Coast, Savannah and Sahel, was analyzed. The potential change associated with global warming is assessed by the pseudo global warming (PGW) downscaling method. Multiple PGW runs were conducted using climate perturbation from the 40-member ensemble of the Community Earth System Model version 1 (CESM1) coupled with Community Atmospheric Model version 5.2 (CAM5.2) component large ensemble project. The model output was compared with TRMM and GPCP rainfall and atmospheric parameters from ECMWF reanalysis datasets. Results show that the rainfall amount in the 2070s estimated from the PGW runs substantially increases, especially in the eastern Sahel due to enhanced moisture convergence, compared to the current climate. The percentage change in simulated total rainfall amount can increase or decrease by 50% in the PGW runs and the theoretical rainfall computed based on Clausius-Clapeyron relation. Also, found is an increase (decrease) in heavy (both light and moderate) rainfall amount. These results, however, depend on the GCM used as the boundary conditions of the RCM. This suggests that the 4 ^{o} C change in average surface temperature derived from the 40-member ensemble model strongly influenced the increased rainfall simulated by the PGW experiments. Thus, highlighting the advantage of using the PGW technique to estimate the likely difference between present and future climate with reduced large-scale model biases and computational resources.

Keywords: Rainfall; Temperature; Guinea coast; Savannah; Sahel; Weather Research and Forecasting model; Community Earth System Model; Pseudo global warming

1. Introduction

West African Monsoon (WAM) prevails during the West African rainy season and provides over 75% of annual rainfall (Hagos and Cook, 2007) in most parts of the region. Activities of the WAM vary at intraseasonal, interseasonal and interannual time scales. The emergence of the changing climate, largely ascribed to human-induced anthropogenic activities, can further amplify these variations thereby causing serious consequences for human health and well-being, agriculture and food security, water resources and hydrological cycles (IPCC, 2001, 2007, 2013, 2018). The WAM is prone to large interannual rainfall variability with significant consequences on human and socioeconomic outputs. This is partly due to high dependence on rainfed agriculture, which is already threatened by insufficient rainfall. Therefore, a better knowledge of how climate change will influence the WAM and how such changes will impact socioeconomic outcomes including crop productivity is key to inform policies that may reduce the adverse effects and ensure food security in the region is required (Sultan and Gaetani, 2016). Thus, the need to improve modeling of the monsoon system and to better quantify the uncertainty in its variability under a warming climate.

Assessment of the past and future climate is therefore necessary to understand how the monsoon region has responded to these changes and how the changes will likely manifest in the future. This process is quite important to provide climate science basis to guide climate action in order to ensure improved societal benefits. Sound climate science basis partly require inference derived from the analysis of outputs from fully-coupled community atmospheric and global circulation models (GCMs). GCMs are useful tools with complex non-linear mathematical equations that describes the major climate system components (e.g. atmosphere, land surface, ocean, and sea ice), and their interactions. These state-of-the-art models can be employed to investigate climate change associated with increase in greenhouse gases caused by anthropogenic activities as well as the change caused by changes in natural processes that occur within the climate system. However, the coarse nature of GCMs horizontal resolution limits their ability to reproduce local climates, which are directly related to their inability to properly resolve orographic features (IPCC, 2007; Lupo et al., 2013, among others). Other methods such as statistical downscaling (Schmidli et al., 2006), dynamical downscaling (CORDEX, Giorgi and Gutowski 2015; Akinsanola et al., 2015) and direct simulation by high resolution GCM (Wild et al., 1995) are gaining more application to project climate conditions at regional scale. Also, several studies have shown that regional climate models (RCMs) reproduce the dynamic features of the West African monsoon system and its associated temperature and rainfall patterns, although there are some level of uncertainties linked to parameterization of model subgrid scale processes (Jenkins et al., 2005; Sylla et al., 2013a; Akinsanola et al., 2018). These complex subgrid scale processes directly impact the monsoon system of West Africa. Due to advances in climate modeling interest is now shifting to high-resolution climate change simulation that permits convection and resolves complex mesoscale interactions related to orography and local climate at < 4-km grid spacing (Prein et al., 2013; Marsham et al., 2013; Liu et al., 2017), although this type of simulation can only be achieved with high computational cost. Some regional and global atmospheric model experiments including the African Monsoon Multidisciplinary Analysis (AMMA) Model Intercomparison Project (AMMA-MIP; Hourdin et al., 2010), the West African Monsoon Modeling and Evaluation (WAMME; Xue et al., 2010) project, and the African component of the Coordinated Regional Climate Downscaling Experiment (CORDEX-Africa; Jones et al., 2011; Nikulin et al., 2012) have shown good skills in representing the atmospheric processes in Africa. These models, however, contain large biases in rainfall and meridional circulation (Hourdin et al., 2010; Xue et al., 2010; Boone et al., 2010).

Previous studies have attempted to investigate how the global and African climate will change in the future (e.g. Hulme et al., 2001; Christensen et al., 2007; Giannini et al., 2008; James and Washington, 2012; Biasutti, 2013; James et al., 2015; Monerie et al., 2017; Dunning et al., 2018; Akinsanola and Zhou 2019). These studies employed climate models and found a decrease (increase) in rainfall in most parts of the subtropics (tropics). Further analysis revealed that multi-model agreed in terms of significant regional specific trends of dryness in southern Africa (Shongwe et al., 2009) and wetness in East Africa (Shongwe et al., 2011). However, there are still large uncertainties in the future climate in Sahel (Biasutti and Giannini, 2006; Monerie et al., 2020). These uncertainties are partly due to the complex interactions and processes within the climate system, which are not fully understood and inadequately modeled (Cook and Vizy, 2006; Akinsanola and Zhou 2019; Monerie et al., 2020). Following the outcome of the Paris Agreement, there have been several high-level discussions to keep the global mean surface temperature well below 2 ^{o}C above the preindustrial level (Hulme, 2016). This was accompanied by the recent special report on the impacts of global warming of 1.5 °C above pre-industrial levels and related global greenhouse gas emission pathways (IPCC, 2018). However, the questions on how warming will impact West African climate systems, most especially the monsoon, is widely open to favorable unanimous answers. A clear understanding of the implications of threshold warming and a more extreme scenario case like the representative concentration pathways 8.5 (RCP8.5) is critical for the West African region to device appropriate mitigation and adaptation measures. This imperative orient the current study towards investigating the impact of worst-case scenario RCP8.5 on the monsoon system with focus on rainfall and surface temperature.

Furthermore, the large interannual variability of monsoon rainfall in West Africa underscores the need for long-term dynamical downscaling, such as the CORDEX (Giorgi et al., 2009), or ensemble projects, to investigate how the parameter will respond to warming climate. Outputs from these types of simulations are important for climate impact assessment studies. Currently, it is computationally intensive to produce long-term simulations at several tens of kilometers or even convection permitting grid over large regions such as West African domain. This is partly due to insufficient and high cost of computing resources.

Therefore, an alternative less computationally intensive climate simulation method such as the Pseudo-Global Warming (PGW) technique (Liu et al., 2017) is necessary. The current study demonstrates the usefulness of applying this method to assess climate change impacts through the use of shorter numerical experiments with less computing requirements rather than performing a longer year-to-year simulation with intensive computational needs.

The overall objective of this research is to use the PGW technique to investigate the impact of warming climate on rainfall in West Africa during the monsoon period. This study builds on previous works where sensitivity test was performed to identify good sets of physics combinations that better describe the West African monsoon in Weather Research and Forecasting (WRF) model (Gbode et al., 2019a). In the same study, the WAM rainfall season shows strong sensitivity to the choice of both planetary boundary layer and convection schemes. Also, the WRF RCM proves to be skillful in reproducing the main observed features of the large-scale circulation during wet and dry WAM rainfall periods (Gbode et al., 2019b). Hence, making the WRF model a useful tool for investigating the response of WAM rainfall seasons to warming climate in the future. In the current study, we employed the PGW method to examine the potential role of warming on WAM by directly comparing future rainfall amount with that of the current. Further the study investigates how the effect of warming on rainfall varies in the different climatic zones of the region. The remaining part of the paper is structured as follows, Section 2 describes the study area and numerical experiment setup as well as the observation and reanalysis data used. Results and discussion are presented in Section 3 and the conclusion is drawn in Section 4.

2. Model domain, data and methods

2.1 Model domain and numerical experiment setup

The WRF version 3.8.1 model is used as a common framework to perform the regional climate simulations over a 20 km horizontal resolution with 50 model levels. Similar to the study of Gbode et al. (2019a,b), the domain covers the West African region (0°–20° N, 20° W–20° E; see Figure 1) and parts of the Atlantic Ocean that provides the moisture carried into the region by the monsoon flow. Analysis was done for three climatic zones (Figure 1) including Guinea coast (4-8°N), Savannah (8-11°N), and Sahel (11-16°N). These zones were delineated based on similarities in their zonal characteristics, such as, land use/land cover, climate and ecosystems (Iloeje, 1981; Omotosho and Abiodun, 2007; Abiodun et al., 2013). The activities of the West African monsoon in the zones vary differently in terms of the rainfall amount received and length of the rainy season. Guinea Coast zone is characterized by a sub-humid climate with two rainfall seasons and average annual rainfall ranging from 1575-2533 mm (Oguntunde et al., 2011; Gbode et al., 2019c). The Savannah is a semi-arid region with average annual rainfall of about 897-1535 mm. Rainfall decreases in this region as a direct response to the monsoon jump, an abrupt nonlinear latitudinal shift of maximum rainfall from the Guinea coast to the Sahel zone in June (Sultan and Janicot, 2000; Le Barbe et al., 2002; Lebel et al., 2003; Hagos and Cook, 2007). Sahel displays a single rainy season covering July to September with a pronounced peak in August which coincides with the northernmost position of the Inter-Tropical Discontinuity (ITD) at about latitude 21-22° N (Nicholson, 2013). The average annual rainfall in the region falls between 434 and 969 mm (Oguntunde et al., 2011; Gbode et al., 2019c).

The study analyzed five years with different characteristics in terms of rainfall amount in order to account for interannual variability. The considered years represents wet (2008 and 2010), dry (2001 and 2011) and normal (2007) monsoon years. The characteristics of the chosen years are determined by the departure of the total annual rainfall amount from long-term mean annual rainfall over the entire West African domain (Not shown for brevity, similar to Klein et al., 2015; Gbode et al., 2019b).

The numerical study includes three sets of model experiments each for present and PGW simulations. These experiments combine two different WRF model microphysics (MP), three planetary boundary layer (PBL) and three cumulus convection (CU) parameterization schemes: i) Goddard (GD) MP, Mellor–Yamada–Janjic (MYJ) PBL and Bett-Miller-Janjic (BMJ) CU (hereafter GD-MYJ-BMJ); ii) Weather Research and Forecasting (WRF) model Single-Moment 5-class (WSM5) MP, Mellor–Yamada–Nakanishi–Niino (MYNN) Level 2.5 PBL and new Tiedtke (nTDK; Tiedtke 1989; Zhang et al. 2011) CU (hereafter WMS5-MYNN-nTDK); iii) WSM5, Yonsei University (YSU) PBL and new Simplified Arakawa Schubert (nSAS) CU (hereafter WSM5-YSU-nSAS). The difference between the two MP schemes used is that WSM5 does not allow supercooled water and has immediate melting of snow below the melting layer while GD is a six-class microphysics with graupel and modifications for ice/water saturation based on Lin et al. (1983). The selected YSU PBL has a stronger boundary layer top entrainment and boundary layer inner mixing than MYJ (Zhang et al. 2012). MYJ is a local closure scheme that predicts

turbulent kinetic energy (TKE) while MYNN uses local TKE-based vertical mixing in boundary layer and free atmosphere. The BMJ CU is a profile adjustment scheme that relaxes both deep and shallow profiles to a reference profile without explicit updraft, downdraft, or cloud entrainment. The nTDK is a mass flux scheme with updrafts, downdrafts, entrainment, and detrainment of cloud, rain, ice, and snow. It has both deep and shallow convections and uses a convective available potential energy (CAPE) removal time- scale closure. nSAS is another recently modified scheme with CAPE removal timescale that has momentum transport with a pressure term and new mass flux type shallow convection that is different from the earlier SAS CU. The choice of the selected combinations is based on results from a previous study (Gbode et al., 2019a) in which the first two combinations were categorized as good physics options and the last configuration as a moderate option based on comparative model skill score.

Basically, two sets of experiments were performed to represent the current and PGW climate. The first experiment was a retrospective simulation aimed at reproducing the variability and mean state of the current climate within the model domain. The current climate simulation contains the selected years from January 1 to December 31 but the analysis focused on the period March 1 to October 31, during which the rainfall accompanying the monsoon become more frequent and intense. The present climate runs were hindcast runs using 6-hourly ERA-Interim (ERAI, Dee et al., 2011) atmospheric data with soil initialization (soil moisture and temperature) from National Centers for Environmental Prediction Final Reanalysis (NCEP FNL, 2000) (Equation 1). The NCEP FNL soil data was kept constant in all simulation because it is consistent and adequate with the unified Noah land surface model as shown by Gbode et al. (2019a).

$$WRF_{Input1} = ERAInterim_{Atmosphere} + FNL_{Soil} \quad (1)$$

2.2 Pseudo-global warming simulation

The PGW approach (Kimura and Kitoh, 2007; Sato et al., 2007; Hara et al., 2008; Rasmussen et al., 2011, 2014; Liu et al., 2017) is a dynamic downscaling method that permits regional climate change projections with the use of a regional climate model. The PGW method employs initial and lateral boundary conditions that combine 6-hourly reanalysis data and the climate change signals, which are the monthly averaged differences between the current and future climate projections produced by a GCM. The method expects the boundary condition mean state to have similar climatology to those of the GCM future climate projections, but the daily evolution is similar to that of current years. The PGW technique provides the possibility of having a direct comparison between the present year and the PGW year in the context of the interannual variation with the addition of future climatology.

Another set of simulations that closely follow the PGW approach was performed. Though, the approach doesn't account for extreme events, it however allows direct comparison between the current and future climate. The selected 5-year simulations were forced with ERA-Interim, FNL reanalysis plus climate perturbation (see Equation 2) derived from the Community Earth System Model version 1 (CESMv1) with the Community Atmospheric Model version 5.2 (CAMv5.2) of the Large Ensemble Community Project (LENS) (Kay et al., 2015). The LENS CESMv1-CAMv5.2 is approximately 1° latitude/longitude with CAMv5.2 as its atmospheric component. CESMv1-CAMv5.2 is a 40-member ensemble of the LENS of fully-coupled CESMv1 simulations for the current (i.e. historical) and future (i.e. RCP8.5) periods 1976-2005 and 2071-2100, respectively. Each member is subjected to the same radiative forcing scenario but begins from a slightly different initial atmospheric state created by randomly perturbing temperatures at the level of round-off error (Kay et al., 2015). The ensemble average is used to remove interannual variability from the climate-change signal (Annan and Hargreaves, 2011).

$$WRF_{Input2} = ERAInterim_{Atmosphere} + FNL_{Soil} + \overline{\Delta CESM1\_CAM5.2_{RCP8.5}}^{monthly} \quad (2)$$

where $\overline{\Delta CESM1\_CAM5.2_{RCP8.5}}^{monthly}$ (Equation 3) is the 30-year monthly mean change signal derived from the LENS 40-member ensemble under the business as usual representative concentration pathway (RCP8.5), a comparatively high greenhouse gas emission pathway (Riahi et al., 2011). The technique benefits from reduced biases and uncertainties of an individual realization by using multiple simulations from the single GCM in order to improve the projections (Giorgi and Mearns, 2002).

$$\overline{\Delta CESM1\_CAM5.2_{RCP8.5}}^{monthly} = \overline{CESM1\_CAM5.2_{2071-2100}} - \overline{CESM1\_CAM5.2_{1976-2005}} \quad (3)$$

The perturbed physical fields include horizontal wind, temperature, relative humidity, sea surface temperature and sea level pressure. First the climate change signals are obtained at monthly-average resolution and then these are interpolated to reanalysis times (i.e. from monthly to 6 hourly time steps) and to the model grid when adding them to the reanalysis.

Before running the PGW simulations, the WRF model was recompiled to reflect the expected mean greenhouse gas (GHG) concentration levels of the mid-year of the last climate epoch of the 21st Century (2086) for the (RCP8.5, see Table1; IPCC, 2007, 2014).

Furthermore, the theoretical precipitation change based on the Clausius-Clapeyron (CC) relation that describe the rate of change of saturated water vapor with temperature was analyzed. The CC expression for the saturation vapor pressure (e_s) is given as (Equation 4):

$$\frac{d \ln e_s}{dT} = \frac{L}{RT^2} = \alpha(T) \tag{4}$$

where L is the latent heat of vaporization and R is the gas constant. Within the lower troposphere the saturation vapor pressure increases by about 7% for each 1-K increase in temperature (i.e. $\alpha \approx 7\%\,\mathrm{K}^{-1}$; Held and Soden, 2006; Martinkova and Kysely, 2020). Therefore, if the equilibrium response of lower tropospheric temperatures to an increase in GHG concentration is close to the canonical mean value of 3 K, the e_s will increase by 21% (Held and Soden, 2006). The approximation of 7% per K is based on the assumption that all factors influencing precipitation remains constant and, thus, precipitation will be proportional to the amount of water that is held in the atmosphere. Besides, the rate of change of e_s with T may as well be the rate of change for the most intense precipitation events with T (Allan and Ingram, 2002).

Based on these discussions, the theoretical change in precipitation as a result of change in temperature between the PGW and current climate is computed using the expressions in Equation 5;

$$\%\,\Delta\, Precipitation = \alpha \times \Delta\, Temp \times Precipitaion_{Current} \tag{5}$$

where $\Delta\, Temp$ is the temperature change between the PGW and current climate (Equation 6).

$$\Delta\, Temp = Temp_{PGW} - Temp_{Current} \tag{6}$$

In addition, the vertically integrated moisture flux convergence (VIMFC) is computed. The VIMFC (Equation 7) basically consist of two terms proportional to the convergence of the horizontal wind vector and to moisture advection, also referred to as "moisture pooling" (Van Zomeren and Delden, 2007). The value of the first term often dominates and it is associated with forced lifting. The VIMFC takes into consideration factors necessary for convection.

$$VIMFC = -\frac{1}{g}\int_{300\ hPa}^{1000\ hPa}\left(\frac{\partial uq}{\partial x} + \frac{\partial vq}{\partial y}\right) dp \tag{7}$$

where u and v are the x- and y-components of the wind velocity, respectively, and other variables remains the same as in the above equations. VIMFC is calculated by summation of the horizontal moisture flux convergence between the 1000 – 300 hPa.

2.3 Datasets

In absence of richly dense network of conventional rain gauge and synoptic weather station, model validation was done against satellite rainfall products (SRPs) and reanalysis datasets. For rainfall, Tropical Rainfall Measurement Mission (TRMM; Huffman et al., 2007) and GPCP (Huffman et al., 2009, 2016) were used. Though the satellite-derived rainfall contains differences due to the different observation platforms and algorithms used in producing them, they however converse the observed mean rainfall characteristics (Sylla et al., 2013b; Noble et al., 2017). The Global Precipitation Climatology Project 1° Daily (GPCP 1dd) is a reliable SRP produced from optimized merged estimates computed from microwave, infrared, and sounder data observed by the international constellation of precipitation related satellites and precipitation gauge analysis (Huffman et al., 2009, 2016). Also, the daily TRMM 3B42

version 7 is another reliable source for merged high-quality precipitation estimates (Huffman et al., 2007). For surface air temperature and other atmospheric parameters, monthly mean of the fifth generation European Centre for Medium-Range Weather Forecasts Re-Analysis (hereafter ERA5; ERA5 2019) data is used. ERA5 combines observations into globally complete fields using the laws of physics with a four-dimensional variable (4D-Var) data assimilation method. ERA5 provides hourly estimates for a large number of atmospheric, ocean-wave and land-surface quantities with a regular horizontal grid of 0.25 degrees at near surface and 37 pressure levels from 1000hPa to 1hPa. The model rainfall is compared with both GPCP and TRMM and its surface air temperature, specific humidity and winds are compared against reanalysis data from ERA5.

3. Results and discussion

3.1 Climate perturbation analysis

This Section examines the climate signals derived from the RCP8.5 LENS CESMv1-CAMv5.2 GCM output by analyzing the climate signals produced from the difference between the two climate periods, that is, current (1976-2005) and future (2071-2100). As mentioned earlier in Section 2.2, the perturbed parameters include horizontal wind, temperature, relative humidity, SST, and sea level pressure.

Figure 2 shows the spatial distribution of the surface air temperature change derived from the difference between the two climate periods from January to December. The figure describes how the surface air temperatures varies and evolve between the two climates. Generally, the values of temperature changes are positive and range between 1-6^{o}C across most months except in September where the upper limit of change is less than 5^{o}C. These values fall within similar range presented in Roehrig et al. (2013). Lower temperature exists over the Ocean while heterogeneous values of higher temperature dominates the entire continent. In January, wide spread of high temperature between 4.5-6^{o}C dominates north of latitude 10^{o}N over land. This pattern intensifies in February thereby creating a belt of high temperature difference (i.e. 6^{o}C and above, as shown in Figure 2b) in regions north of 5^{o} to 10^{o} N latitudes. In March, the widely spread temperature changes becomes more stratified and significantly weakens (strengthens) over the eastern (western) Sahel region. This evolution progresses further in March through to July and August, where a distinct region of maximum warming resides mostly around western Sahel and minimum around eastern Sahel, which is obvious in August (Figure 2). The maxima in western Sahel weakens in September as minimum values advance in the area from the eastern region. Higher values emerge between the latitude bands of 15-20^{o}N in October. This warming intensifies in November where temperature difference of about 6^{o}C dominates most land areas to the north of 15^{o}N. In December the values decrease slightly and extends southwards of the West African region (Figure 2l).

Figure 3 presents the spatial distribution of relative humidity change between the two climate periods from January through to December. Changes in this parameter range from -10% to 10% across land areas. Over the Ocean wetness of 8% or less exists. The evolution of the relative humidity is tightly coupled with the spatial distribution of temperature changes found in Figure 2, which is expected because the two parameters depend on each other, that is, high temperature will result in low relative humidity and vice versa for the same amount of water vapor in the atmosphere at a fixed pressure level. For example, regions of dryness correspond with region of intense warming in the western Sahel. In January and February there exists a zonal positive difference close to the south coast of the region. Based on relative humidity, the continent appears to be dryer in the future projection from March through to August, during which the WAM appears and dominates the West African region. In March, a region of dry maxima emerges and becomes well defined in May as it intensifies and progresses north approximately from latitude 11^{o}N to 16^{o}N in August. A region of wetness resides along 15^{o}N in October. This region of positive values weakens and advances southwards in November and even further in December.

The differences in wind vector, temperature (red contour) and relative humidity (filled contour) at 850mb pressure level is presented in Figure 4. At this pressure level, north easterly trade winds usually dominate during January to March as well as in October to December while the south easterlies trade winds appear in April and dominate through to September. Wind speed difference of about 1.2ms^{-1} exists between the two climates. Away from the monsoon months (January-February and October-December) the changes are negative mostly over the Ocean and large land area (Figures 4 a, b and j-l). Positive wind speed difference appears from March to September, when it becomes enhanced and widely spread over land areas. Away from the WAM season are south westerly anomaly wind flow consequently to weak north easterlies anomaly in the future climate, there exits north westerly difference to the south of 10^{o}N during the monsoon months. At this level region of positive temperature changes coincide with region of low

relative humidity changes as found in Figures 2 and 3. Likewise, areas of positive wind speed changes correspond with warm areas while negative values are associated with positive relative humidity changes.

At 600mb, where the African Easterly Jet (AEJ) resides, the winds are usually easterlies and intensifies as they evolve from January to August, where the AEJ attains its maximum latitudinal position of approximately 16^{o}N, thereafter recedes and weakens in September and beyond. The wind speed difference at this level approximately ranges between -2.5ms^{-1} and 2.5ms^{-1} (Figure 5). In the same figure, the moisture and temperature difference strongly couple with each other. Areas of negative relative humidity change correspond with the region of maximum temperature difference in April to August (Figures 5 d-h). Projected wind speed is weak relative to the current climate from January to March, especially over the Sahel in March. Similarly, the winds are also weak from September to December in the future climate. In March, positive wind speed difference begins to appear and intensify further in April thereafter dominating the entire West African region from May to July. The positive change weakens and moves further north as the negative changes begin to emerge over the Ocean and eastern corner of the region in August (Figure 5h). The negative wind speed difference strengthens and dominates larger land area in September before becoming less strengthened in the successive months. The wind vectors at this level are consistent with the easterly flow as the difference produce anomalous easterlies, especially during the monsoon periods, but westerlies are found around regions with negative wind speed, when the future wind speed are weak.

Another pressure level critical to the West African climate system is the 150mb where the Tropical Easterly Jet (TEJ) resides. At this upper tropospheric level, the winds are predominantly westerlies in January-March and October-December. In April, the easterlies begin to emerge gradually from the southern coast of the region before becoming prevalent in May through to September (not shown for reasons of brevity). This enhances the upper level divergence that encourages the uplift of lower-level air and enhancing a surface low beneath to create a favorable condition for the WAM to thrive. Winds found at this level is stronger compared to that at 600mb. The difference between the current and future climate obtained from the CESM data reveals changes of about 10ms^{-1} (Figure 6). Far north, the wind vectors are mostly westerly anomaly but anomalous easterlies to the south and over areas closer to the coast between January-March. The anomalous westerlies intensify from May to June but weaken over land areas in July. Simulated easterlies in the future climate appear to be stronger than the current climate in August and September.

Generally, the future climate is warmer than the current climate and the temperature difference can reach 5.2 ^{o}C. Also, the future climate can be dryer in terms of relative humidity compared with current climate, most especially in the dry season months over Sahel region, however, positive changes reaching 6% can also be found over ocean and land areas across the months.

3.2 Temperature characteristics

Temperature distribution is a very important measure that determines the state of the climate system and variations in their spatial pattern can offset regional monsoon activities as well as climate-sensitive functions such as human health, ecosystem and others (Mc Michael et al., 2003). Regional and local temperature changes vary in space and time therefore the need to investigate these variations between the current and future climate. Figure 7 depicts the mean surface air temperature distribution averaged during the period March-October for ERAI reanalysis and model outputs (i.e. present and future runs). In this panel, Figures 7a, d, g, and j shows the current runs from CESM and WRF, Figure 7m depicts ERAI, Figures 7b, e, h, and k show the future CESM and PGW runs, and Figures 7c, f, i, and l, depicts the difference between future and present climate.

The reanalysis shows temperature range between 20-36^{o}C with steep gradient in the Sahel. This gradient is associated with the Saharan heat low defined by the mean position of the Inter-Tropical Discontinuity (ITD) and low-pressure center, an obvious feature in August when the monsoon is fully developed (Nicholson, 2013). Also, surface air temperature over complex orographic terrains is cooler relative to the desert and nearby land areas. During the 20th century (Figure 7a), CESM simulates similar spatial temperature distribution as observed with lower values over complex terrains, mostly over the Jos Plateau, Cameroun Mountains and Fouta Jallon highlands, and eastern Sahel region. In the future runs (Figure 7b), the model simulates warmer conditions over the complex terrains and even higher temperatures of about 40^{o}C over the western Sahel. The current climate runs from the WRF model (Figures 7d, g, j) also agree with the reanalyzed spatial temperature distribution but with some biases mostly in the Sahara desert region, thereby highlighting the model weakness which can be partly explained by the role of

the PBL used (Flaounas et al., 2011) and surface processes. Simulated air temperature in the PGW runs, generally, shows intensified warming over ocean and most land areas, particularly in areas north of 10°N (Figures 7e, h and k). The maximum value exceeds 40°C over the desert area. Relative to the present climate, the PGW runs could be 5°C warmer in some land areas (Figures 7f, i, and l). In GD-MYJ-BMJ8.5 and WSM5-YSU-nSAS8.5 there is a uniform warming of 4°C from the coast upward to about 15°N latitude followed by a northward steep gradient. Similar warming pattern is found in WSM5-MYNN-nTDK8.5 but restricted only to about 10°N. Over the ocean, the magnitude of warming is lesser perhaps due to its high heat retention capacity.

The distribution of temperature values during the period March-October for areas enclosed within latitudes 5°-15°N and longitudes 10°W-10°E shows values between 25°-31°C in ERAI with the mean being 27.9°C (Gbode et al., 2020). The distribution of the current climate simulation ranges from 24°-31.5°C. Relative to the WRF simulations, CESM simulates lower temperatures during the current and future runs. GD-MYJ-BMJ distribution simulates average values closer to that of the ERAI. WSM5-MYNN-nTDK produces a lower mean of about 0.4°C while the WSM5-YSU-nSAS a warming of about 0.6°C relative to ERAI. PGW runs predicts wider range of temperature (28°-36°C) and a significant shift in the mean (Gbode et al., 2020). The average difference in the mean between the PGW and current could reach 4°C and above (Figures 7f, i and l). The warming introduced by the GCM used and the change in GHG concentration in the WRF model (Table 1) is found to generally influence all three simulations. This temperature value lies within the range of warming found with RCP8.5 for the period 2071-2100 over Kenya (Muhati et al., 2018). Though the WSM5-YSU-nSAS8.5 shows higher surface temperature mean and range, the differences in mean between the current climate remains below 6°C. This could explain the higher values of rainfall amount found in the combination (Table 2 and Figure 8) as increasing temperature will favor surface evaporation, which in turn will enhance convective activity. The temperature range of WSM5-MYNN-nTDK8.5 is smaller compared to GD-MYJ-BMJ8.5 but the two combinations have almost the same mean value (as shown in Gbode et al., 2020).

CESM simulate lower temperatures compared to ERAI and WRF current and PGW runs. This underscores the benefit of having a high-resolution regional climate simulation (Prien et al., 2013). The three model experiments also reproduced the observed distribution with varying density. For example, the density of low temperature values in WSM5-MYNN-nTDK is higher compared to GD-MYJ-BMJ and WSM5-YSU-nSAS (Gbode et al., 2020). During the last climate regime of the 21st Century (2071-2100), both GCM and RCMs simulates significant increase in temperature.

3.3 Rainfall characteristics

Surface warming is directly coupled with increase in rainfall because warming effect intensifies evaporation processes over ocean and water body surfaces and increases the water-retention capacity of the atmosphere as described by Clausius-Clapeyron equation (Xiang, 2005; Held and Soden, 2006; Martinkova and Kysely, 2020). Therefore, increasing surface temperature associated with global warming will indeed influence the spatial pattern and distribution of rainfall received in the West African region. Figure 8 presents the observed average daily rainfall amount (Figures 8m and n) and the modeled values for current climate (Figures 8d, g and j) during the period March to October. The Figure also presents the rainfall percentage difference relative the PGW (Figures 8e, h and k) and CC relations (Figures 8f, i and l). GPCP and TRMM (in Figures 8m and n) show average daily rainfall values reaching 14 mm day^{-1} and 16 mm day^{-1}, respectively. Both SRPs agree in terms of producing maximum values over complex orographic terrains and minimum in other land areas. Though CESM simulate values of 16 mm day^{-1} in the 20th Century (Figure 8a) and RCP8.5 (not shown) in agreement with TRMM, it however show deficiencies in reproducing the observed maximum over complex terrains of Jos Plateau and the southeast orientation pattern over the Cameroun Mountains. This points out the limitations of the GCM in reproducing certain features due to its coarse horizontal resolution. This limitation makes it difficult for GCMs to properly capture atmospheric phenomena at smaller horizontal scales than its grid (IPCC, 2007; Lupo et al, 2013, among others).

The RCM runs agree with observations as they simulate the climatological rainfall maxima over complex orographic terrains of Cameroun Mountains, Jos Plateau, and Fouta Djallon highlands with extension towards the west coast of West Africa. In the present year simulations, GD-MYJ-BMJ also reproduces the magnitude of 16 mm day^{-1} over the Cameroun Mountain and the west coast of the monsoon region (Figure 8d). For WSM5-MYNN-nTDK and WSM5-YSU-nSAS (Figure 8g and j) runs the simulated magnitude reaching 15 mm day^{-1}. The PGW runs shows increase in daily rainfall relative to the present

climate runs, especially over complex orographic terrains and over the west coast of West Africa. While the simulated values of GD-MYJ-BMJ8.5 and WSM5-YSU-nSAS8.5 could be greater than 17 mm day^{-1}, WSM5-MYNN-nTDK8.5 only simulates a maximum of 15 mm day^{-1} (not shown for brevity).

Although the models agree with the observed rainfall patterns, there exist some systematic errors. However, the percentage difference between the PGW and current climate show negative and positive rainfall change of about 50%. This change is seen to be more pronounced in the Sahel region where surface temperatures are highest. Also, consistent in the RCMs and GCM are region of dryness over western Sahel region, as found in previous studies (e.g. Biasutti, 2013). The theoretical rainfall computed based on the CC relation show a general increase of rainfall up to 40%. Though this highlights the significant role of surface temperature on convective processes, the approximation is, however, based on the assumption that all factors influencing precipitation must remain constant for precipitation to be proportional to the amount of water that is held in the atmosphere (Allan and Ingram, 2002). In general, the average percentage difference is greater, especially in Sahel suggesting the possibilities of greater impact of global warming on rainfall activities in Sahel (e.g. Akinsanola and Zhou 2019; Monerie et al., 2020). Relative to the Sahel, where the land surfaces are pseudo homogenous, lesser impact is expected in the Guinea Coast, where there are heterogeneous surfaces and local features, and a mild influence in Savannah. Further inference from this result suggests that homogenous surfaces would respond to warming at a degree greater than heterogeneous surfaces and thus its impacts on atmospheric phenomenon such as rainfall. The impact of warming is, therefore, evident through increase in the mean rainfall of PGW runs. This result agrees with the findings of Maynard et al. (2002) where model project enhanced rainfall associated with WAM at the end of the twenty-first century, which is linked to changes in precipitable water, water vapour recycling, moisture convergence and rainfall efficiency. Other studies also reported varying patterns of rainfall in the West African region in a warming climate, specifically noting more severe drought conditions over western Sahel and an increase in rainfall in the central Sahel (for example Biasutti, 2013; James et al., 2015; Monerie et al., 2017; Dunning et al., 2018; Akinsanola and Zhou 2019). These uncertainties in the model results can be partly attributed to the differences in atmospheric circulation simulated by the models over West Africa (Monerie et al., 2020).

Table 2 shows the total amount of rainfall received from GPCP, TRMM, and WRF model for each climatic zone from March to October. On the Table, wet and dry years are consistent in GD-MYJ-BMJ for both current and PGW simulations in all the three climatic zones (Guinea Coast, Savannah and Sahel) outlined in Figure 1. This agreement between GD-MYJ-BMJ and observations highlights its skills in simulating realistic rainfall amount during the considered period. In WSM5-MYNN-nTDK, the rainfall amount for the simulated years is well defined only in Savannah and Sahel in both periods but not distinctly defined in WSM5-YSU-nSAS runs. Further, WSM5-YSU-nSAS simulates higher rainfall amount compared to the other two experiments.

To further investigate the characteristics of daily rainfall over the region, the rainfall is divided into different categories; light (1-2 mm day^{-1}), moderate (>2-10 mm day^{-1}) and heavy (>10 mm day^{-1}), based on the probability density function (Gbode et al., 2020). Figure 9 shows the total rainfall and percentage contribution derived from light rainfall intensity for the period March to October. Observed and simulated total rainfall in this category could averagely reach 200 mm. GPCP and TRMM (Figures 9a and b) show that daily rainfall within this range provides 9.1 % and 8.4 % of rainfall, respectively, during the considered period. Most of the rains in this category are received within 10^{o} W – 10^{o} E longitudes and extends to 15^{o} N latitude and along the southern coast of the Atlantic Ocean. Also, the rains are observed to spread over complex terrains like the Cameroun Mountains, most obviously in TRMM. The WRF simulations (Figures 9c-h) also agree with the observed spatial pattern and provide percentage of rainfall between 7.7 - 8.7 %, which lies within the observed range. Though analysis of the density distribution (in Gbode et al., 2020) shows that the rainfall in this category slightly increase, the percentage contribution is expected to decrease by 0.8-1 % in GD-MYJ-BMJ and WSM5-YSU-nSAS while no change is found in WSM5-MYNN-nTDK. Total amount of rainfall in the range of 1-2 mm simulated by CESM (Figures 9i and j) provides more widely spread spatial pattern along the Sahel and the southern coast of the Atlantic. Similar to the WRF runs, the GCM simulates percentage decrease of 0.8 % and much less contribution of this type of rainfall for some areas along Guinea coast.

Rainfall within 2-10 mm provides the most widely spread values, that is, mean observed amount of 1250 mm in the monsoon region. This rainfall category provides 71.7 % and 51.6 % of rainfall in GPCP and TRMM (Figures 10a and b), respectively. The percentage contribution of rainfall in this category lies

between the observed values in the current climate simulation (Figures 10c-e). WRF PGW runs (Figures 10f-g) show not only a decrease in the frequency of rains in this category but also a decrease in the percentage (i.e. 3-6 %). Also, the mean rainfall amount can possibly reach 1500 mm. CESM (Figures 10i and j) simulates a percentage decrease of 6.5 % in the future runs and this type of rains provides virtually all the rainfall over most parts of the Guinea Coast.

Figure 11 depicts the total amount and percentage of heavy rainfall received in the monsoon domain. Heavy rainfall (i.e. 10 mm and above) contributes 19.1 % and 40 % of rainfall is observed in GPCP and TRMM (Figure 11a and b), respectively. The mean of the total rains received from this category is 2500 mm and it mostly occurs over complex terrains, especially over Cameroun Mountains and west coast of West Africa. Other areas of the region also receive rainfall from this category but at far lesser amount. WRF runs (Figures 11c-h) also agree with observations, mostly over the complex topographic terrains. In the PGW runs, the percentage of this type of rainfall is expected to increase by 3-6.5 %. For CESM (Figures 11i and j), 42.2 % and 49.4 % is simulated in the current and future climate, respectively. The GCM simulates this feature only in the complex terrain of Cameroun Mountains and west coast of the monsoon region.

Furthermore, the model's total rainfall is divided into non-convective and convective rains in order to quantify the contribution of cumulus (CU) and microphysics (MP) physics (shown in Table 3). The CU schemes are responsible for the convective rainfall while the MP schemes produce the non-convective rainfall. This analysis is performed to investigate the influence of these schemes in each of the three configurations over the three climatic zones and the monsoon region. On average, GD-MYJ-BMJ combination produced approximately 60% and 40% of convective and non-convective rainfall, respectively. In the Guinea coast, convective rainfall contributes about 75% of the total rainfall. In WSM5-MYNN-nTDK and WSM5-YSU-nSAS, convection provides about 85% of the simulated rainfall in all climatic zones. The results highlight the dominating role of mass flux convection schemes (i.e. nTDK and nSAS) on the WSM5 microphysics schemes. However, both CU and MP schemes provides considerable amount of rainfall in the GD-MYJ-BMJ combination. Although the profile adjustment convection scheme (BMJ) simulates less rainfall compared with mass flux schemes, it however reproduces realistic total rainfall amount. Therefore, it can be inferred that convective processes are very critical to model rainfall generation in the monsoon region and thus the relevance of ensuring accurate representation of convection and other important sub-grid scale processes in the model.

3.4 Dynamics and thermodynamics feedback

The West African climate system varies over difference time scales ranging from intraseasonal, interseasonal, interannual, to interdecadal. The climate can vary as a result of complex thermodynamic processes that are directly related to heat, moisture and momentum exchanges within the atmospheric column and partly related to anthropogenic activities that alter the GHG concentrations (e.g. CO_2). It is, therefore, necessary to analyze the role of various physical atmospheric processes in determining the magnitude of the climate response to a specific forcing. This is required to understand the climate and climate change of the region. This section therefore presents analysis of the dynamics and thermodynamics characteristics inherent during the peak of the monsoon rainfall season (i.e. June to September), when the Tropical Easterly Jet (TEJ) and African Easterly Jet (AEJ) are well-defined in ERA5 and in the current and PGW climates. The analysis focuses on the vertical profiles of temperature, zonal-winds and moisture that defines the environment for initiation of convective activities (e.g., Attada et al., 2015, 2020; Martínez-Castro et al., 2017). The combination of the PBL, CU and MP schemes plays a crucial role in the distribution of moisture, heat and momentum within the atmospheric column (Gbode et al., 2019a). Particularly, the PBL defines the profiles of the atmospheric parameters, the CU resolves areas of instabilities to produce convective precipitation while the MP remove excess precipitable water in terms as grid-scale precipitation.

Vertical profiles of some observed and modeled atmospheric variables averaged over latitude band 5-15^{o}N and longitude band 10^{o}W – 10^{o}E area for the period JJAS are presented in Figure 12. As expected, temperature increase with height in ERA5 and model (Figure 12a). The modelled temperature profiles in the current climate are similar compared to ERA5. For the PGW runs, the atmospheric column appears to be, on average, about 2-3^{o}C warmer in all model combination. Also, all the models simulated temperature inversion at the surface, which is consistent with results found in the spatial distribution of temperature (Figure 7). In general, the model's temperature profile compares well with observation in the current climate simulation. However, there exit differences that are less than 1^{o}C. Noticeable are the slight

difference found within lower troposphere, where ERA5 is colder than models below 800hPa and above level where the models produced inversion. Also, in the lower troposphere, WSM5-MYNN-nTDK is found to be colder relative to WSM5-YSU-nSAS and GD-MYJ-BMJ combinations in the two climate regimes. The models also compare well with the observed moisture profile (Figure 12b), although with some notable differences which could be as high as 3g kg^{-1} at the surface and less that 1g kg^{-1} in the upper troposphere. Relative to ERA5, moisture in the model are drier from surface to about 800hPa and wetter above 750hPa to approximately 300hPa, where the atmosphere becomes drier in both observation and model. WSM5-MYNN-nTDK appears to have more moisture within the lower and middle tropospheric column (i.e. from surface to about 650hPa) in the current and PGW climate. Above 650hPa, the values are slightly different among models. The structure of the observed (ERA5) zonal wind profile (Figure 12c) clearly defines the presence of the low-level monsoon flow maximum at around 925hPa, the AEJ at 600hPa and TEJ at approximately 150hPa. These features are also simulated by the models but with varying magnitudes. An obvious difference is the strong monsoon flow produced by the models at low-level. Though all models agree with the observed core position of the AEJ (i.e. 600hPa; ~8 ms^{-1}), they differ in terms of magnitude. The AEJ is strongest in WSM5-YSU-nSAS (~11 ms^{-1}) and weakest in GD-MYJ-BMJ (~9 ms^{-1}). Apart from GD-MYJ-BMJ that produced a lower but stronger core of TEJ (~13 ms^{-1}) at 200hPa, the other two combinations produced TEJ at the same level as ERA5. The magnitude of TEJ is less in WSM-YSU-nSAS relative to ERA5. Overall, the magnitude of the simulated monsoon flow and the two middle and upper level tropospheric jets are, however, intensified in. the PGW runs.

Further analysis to examine moisture source region that favour the initiation of moist convection and associated rainfall over the monsoon region was performed using the average JJAS vertically integrated moisture transport (i.e. VIMFC integrated from 1000hPa to 300hPa; Figure 13). Although similar but weaker compared to models, ERA5 shows regions of moisture convergence (divergence) over complex terrains and the western Atlantic Ocean (land areas). Similar patterns of observed moisture transport phase were also produced in the models. The magnitude of convergence and divergence appears to be stronger in the models. The signals in GD-MYJ-BMJ is more intense, especially over the western Atlantic Ocean, compare to WSM5-MYNN-nTDK and WSM5-YSU-nSAS. Most dominant in the PGW runs is the extensive region of convergence around the central and eastern Sahel, which explains the reason why all the models simulate more rainfall over eastern Sahel and less over western Sahel in the future climate (as shown in Figure 8).

4. Conclusion

The impact of global warming on the West African monsoon rainfall amount were examined using the PGW technique. The study compared results from three experiments that combine MP, CU and PBL parameterization schemes for both current and PGW climate runs. Five monsoon seasons, including two wet (2008-2010), two dry (2001-2011) and one normal (2007) year, was simulated over the monsoon region at 20km horizontal resolution. Also, the rainfall characteristics over the three climatic zones, Guinea Coast, Savannah and Sahel, were analyzed. The current and PGW climate runs showed good agreement with the observed rainfall in reproducing the spatial distribution pattern over complex orographic terrains. The rainfall amount in the 2070s estimated by the PGW runs substantially increases relative to the current climate runs. The percentage change in simulated total rainfall amount can increase or decrease by 50% in the PGW runs and the theoretical rainfall (R_{CC}) computed based on Clausius-Clapeyron relation. The difference between current climate runs and observations highlights spatial biases in the model. However, GD-MYJ-BMJ runs have good agreement with observations in terms of simulating the characteristics of wet, dry and normal year monsoon rainfall seasons, which is defined as a function of the total rainfall amount. WSM5-MYNN-nTDK is more consistent in defining the rainfall characteristic in Savannah and Sahel while WSM5-YSU-nSAS rarely agree in any two of the climatic zones. Also, found in the PGW runs is an increase in heavy rainfall amount and a decrease in both light and moderate rainfall amount.

The results of this study are, however, dependent on the GCM, which provides the climate signal used to perturb the boundary conditions for the RCM. Most especially, the temperature change of the GCM which the rainfall amount is sensitive to. CESM1.0-CAM5.2, the GCM employed in this study, tends to provide an average surface temperature change of about 4 ^{o}C from the 40-member ensemble of the LENS project. This increase in surface temperature consequently leads to increase in the simulated rainfall in the PGW experiments and the R_{CC} as it intensifies evaporation that enhances convective activities. The rainfall characteristics presented is, however, limited to the average of the selected 5 years and the RCP used. Also, the role of air temperature on rainfall activity may change for different range of RCPs. Although the PGW

method used in the study further reduces large scale model bias and allows the estimate of climate difference between current and future climate without an ensemble of numerous numbers of simulations, it does not account for extreme events. This underscore the need for longer-term simulations in future studies. Further, it is necessary for future study to consider using the PGW method to downscale the GCM and reanalysis at convection-permitting scale. This approach will, however, ensure that the dynamics of atmospheric convection is treated with sufficient accuracy by switching off parameterization of convective processes in order to reduce associated uncertainties.

Acknowledgments
Our sincere appreciation to NCAR's MMM Laboratory for supporting the research work. We would like to acknowledge high-performance computing support from Cheyenne (doi: https://doi.org/10. 5065/D6RX99HX) provided by NCAR's Computational and Information Systems Laboratory, sponsored by the National Science Foundation. Also, thanks to the anonymous reviewers for the insightful comments and suggestions that helped to improve the quality of the paper.

Conflict of interest
Authors declares no conflicted of interest related to the publication of this manuscript in this journal.

Funding information
The German Federal Ministry of Education and Research (BMBF) primarily funded this research through the Doctorate Research Programme in West African Climate System (DRP-WACS) hosted by the Federal University of Technology Akure (FUTA), Ondo State, Nigeria.

References
Abiodun, B. J., A. T. Salami, O. J. Matthew, Odedokun, S., 2013. Potential impacts of afforestation on climate change and extreme events in Nigeria. Clim. Dyn. 41(2), 277- 293, https://doi.org/10.1007/s00382-012-1523-9

Akinsanola, A.A., Ogunjobi, K.O., Gbode, I.E., Ajayi, V.O., 2015. Assessing the capabilities of three regional climate models over CORDEX Africa in simulating West African summer monsoon precipitation. Adv. Meteor. 2015.

Akinsanola, A.A., Ajayi, V.O., Adejare, A.T., Adeyeri, O.E., Gbode, I.E., Ogunjobi, K.O., Nikulin, G., Abolude, A.T., 2018. Evaluation of rainfall simulations over West Africa in dynamically downscaled CMIP5 global circulation models. Theor. Appl. Climatol. 132(1-2), 437-450.

Akinsanola, A.A., Zhou, W., 2019. Projection of West African summer monsoon rainfall in dynamically downscaled CMIP5 models. Clim. Dyn. *53*(1-2), pp.81-95.

Allen, M.R., Ingram, W.J., 2002. Constraints on future changes in climate and the hydrologic cycle. Nature, 419(6903), 228-232.

Annan, J.D., Hargreaves, J.C., 2011. Understanding the CMIP3 multimodel ensemble. J Clim. *24*(16), 4529-4538.

Biasutti, M., Giannini, A., 2006. Robust Sahel drying in response to late 20th century forcings. Geophys. Res. Lett. *33*(11).

Biasutti, M., 2013. Forced Sahel rainfall trends in the CMIP5 archive. J Geophys. Res.: Atmos. 118(4), 1613-1623.

Boone, A. A., Poccard-Leclercq, I., Xue, Y., Feng, J., de Rosnay, P., 2010. Evaluation of the WAMME model surface fluxes using results from the AMMA land-surface model intercomparison project. Clim. Dyn. **35**, 127–142, doi:10.1007/s00382-009-0653-1.

Christensen, J.H., Hewitson, B., Busuioc, A., Chen, A., Gao, X., Held, R., Jones, R., Kolli, R.K., Kwon, W.K., Laprise, R., Magaña Rueda, V., 2007. Regional climate projections. In *Climate Change, 2007: The Physical Science Basis. Contribution of Working group I to the Fourth Assessment Report of the Intergovernmental Panel on Climate Change, University Press, Cambridge, Chapter 11*, 847-940.

Collins, M., Knutti, R., Arblaster, J., Dufresne, J.L., Fichefet, T., Friedlingstein, P., Gao, X., Gutowski, W.J., Johns, T., Krinner, G., Shongwe, M., 2013. Long-term climate change: projections, commitments and irreversibility. In *Climate Change 2013-The Physical Science Basis: Contribution of Working Group I to the Fifth Assessment Report of the Intergovernmental Panel on Climate Change*, pp. 029-1136. Cambridge University Press.

Cook, K.H., Vizy, E.K., 2006. Coupled model simulations of the West African monsoon system: Twentieth-and twenty-first-century simulations. J. Clim. 19(15), 3681-3703.

ERA5, 2019. ERA5 monthly averaged data on pressure levels from 1979 to present. https://doi.org/10.24381/cds.6860a573

Dee, D.P., Uppala, S.M., Simmons, A.J., Berrisford, P., Poli, P., Kobayashi, S., Andrae, U., Balmaseda, M.A., Balsamo, G., Bauer, D.P., Bechtold, P., 2011. The ERA-interim reanalysis: configuration and performance of the data as- similation system. Q J Roy Meteor. Soc. 137(656), :553–597

Dunning, C.M., Black, E., Allan, R.P., 2018. Later wet seasons with more intense rainfall over Africa under future climate change. J. Clim. *31*(23), 9719-9738.

Flaounas, E., Bastin, S., Janicot, S., 2011. Regional climate modelling of the 2006 West African monsoon: sensitivity to convection and planetary boundary layer parameterisation using WRF. Clim. Dyn. 36(5-6), 1083-1105. https://doi.org/10.1007/s00382-010-0785-3

Gbode, I.E., Dudhia, J., Ogunjobi, K.O., Ajayi, V.O., 2019a. Sensitivity of different physics schemes in the WRF model during a West African monsoon regime. Theor. Appl. Climatol. 136(1-2), 733-751.

Gbode, I.E., Ogunjobi, K.O., Dudhia, J., Ajayi, V.O., 2019b. Simulation of wet and dry West African monsoon rainfall seasons using the Weather Research and Forecasting model. Theor. Appl. Climatol. 138(3-4), 1679-1694.

Gbode, I.E., Adeyeri, O.E., Menang, K.P., Intsiful, J.D., Ajayi, V.O., Omotosho, J.A., Akinsanola, A.A., 2019c. Observed changes in climate extremes in Nigeria. Met. Apps. 26(4), 642-654. https://doi.org/10.1002/met.1791

Gbode, I.E., Ajayi, V.O., Ogunjobi, K.O., Dudhia, J., Liu, C., 2020. Impacts of Global Warming on West African Monsoon Rainfall. In: Leal Filho W., Ogugu N., Adelake L., Ayal D., da Silva I. (eds) African Handbook of Climate Change Adaptation. Springer, Cham. https://doi.org/10.1007/978-3-030-42091-8_93-1

Giannini, A., Biasutti, M., Held, I.M., Sobel, A.H., 2008. A global perspective on African climate. Clim. Chang. 90(4), 359-383.

Giorgi, F., Jones, C., Asrar, G.R., 2009. Addressing climate information needs at the regional level: the CORDEX framework. WMO Bull. 58(3), 175.

Giorgi, F., Gutowski Jr, W.J., 2015. Regional dynamical downscaling and the CORDEX initiative. Annu. Rev. Environ. Res. 4*0*, 467-490. https://doi.org/10.1146/annurev-environ-102014-021217

Giorgi, F., Mearns, L.O., 2002. Calculation of average, uncertainty range, and reliability of regional climate changes from AOGCM simulations via the "reliability ensemble averaging"(REA) method. J. Clim. 15(10), 1141-1158.

Hagos, S. M., Cook, K. H., 2007. Dynamics of the West African monsoon jump. J. Clim., 20(21). 5264-5284, https://doi.org/10.1175/2007JCLI1533.1

Hagos, S.M., Cook, K.H., 2007. Dynamics of the West African monsoon jump. J. Clim. 20(21), 5264-5284.

Hara, M., Yoshikane, T., Kawase, H., Kimura, F., 2008. Estimation of the impact of global warming on snow depth in Japan by the pseudo-global-warming method. Hydrol. Res. Lett. 2, 61-64.

Held, I.M., Soden, B.J., 2006. Robust responses of the hydrological cycle to global warming. J. Clim, 19(21), 5686-5699. https://doi.org/10.1175/JCLI3990.1

Hourdin, F., Musat, I., Guichard, F.S., Ruti, P.M., Favot, F., Filiberti, M.A., Pham, M., Grandpeix, J.Y., Polcher, J., Marquet, P., Boone, A., 2010. AMMA-model intercomparison project. *BAMS. 91*(1), 95-104.

Huffman, G.J., Adler, R.F., Bolvin, D.T., Gu, G., 2009. Improving the global precipitation record: GPCP version 2.1. Geophys. Res. Lett. 36(17). https://doi.org/10.1029/2009GL040000

Huffman, G.J., Bolvin, D.T., Adler, R.F., 2016. GPCP version 1.2 one-degree daily precipitation data set. Research data archive at the National Center for Atmospheric Research, computational and information systems laboratory. doi:https://doi.org/10.5065/D6D50K46

Huffman, G.J., Bolvin, D.T., Nelkin, E.J., Wolff, D.B., Adler, R.F., Gu, G,. Hong, Y., Bowman, K.P., Stocker, E.F., 2007. The TRMM multisatellite precip- itation analysis (TMPA): quasi-global, multiyear, combined-sensor precipitation estimates at fine scales. J. Hydromet. 8(1), 38–55

Hulme, M., 2016. *1.5 °C and climate research after the Paris Agreement.* Nat. Clim. Chang. 6(3), 222–224. doi:10.1038/nclimate2939

Hulme, M., Doherty, R., Ngara, T., New, M., Lister, D., 2001. African climate change: 1900–2100. Clim. Res. 17(2). doi:10.3354/cr017145

Iloeje, N. P., 1981. A New Geography of Nigeria. Longman, UK.

Intergovernmental Panel on Climate Change (IPCC), 2000. *Special report on emissions scenarios (SRES), a special report of Working Group III.* edited by Nakicenovic, N., Alcamo, J., Grubler, A., Riahi, K., Roehrl, R.A., Rogner, H.H. and Victor, N. Cambridge University Press.

Intergovernmental Panel on Climate Change, 2013. *Climate Change 2013: The Physical Science Basis*; Contribution of Working Group I to the Fifth Assessment Report of the Intergovernmental Panel on Climate Change; Stocker, T.F., Qin, D., Plattner, G.K., Tignor, M., Allen, S.K., Boschung, J., Nauels, A., Xia, Y., Bex, V., Midgley, P.M., Eds.; Cambridge University Press: Cambridge, UK; New York, NY, USA, 2013; 1535p.

Intergovernmental Panel on Climate Change, 2014. Climate Change 2014: synthesis report. Contribution of Working Groups I. *II and III to the Fifth Assessment Report edited by* Team, C.W., Pachauri, R.K. and Meyer, L.A., *Geneva, Switzerland*, *151*.

Intergovernmental Panel on Climate Change, 2001. Climate Change 2001: The Scientific Basis. Contribution of Working Group I to the Third Assessment Report of the Intergovernmental Panel on Climate Change, edited by J. T. Houghton et al., 881 pp., Cambridge Univ. Press, New York.

Intergovernmental Panel on Climate Change, 2007. Climate Change 2007: The Scientific Basis. Contribution of Working Group I to the Fourth Assessment Report of the Intergovernmental Panel on Climate Change, edited by S. Solomon et al., Cambridge Univ. Press, New York.

Intergovernmental Panel on Climate Change, 2018. Global warming of 1.5°C. AnIPCC Special Report on the impacts of global warming of 1.5°C above pre-industrial levels and related global greenhouse gas emission pathways, in the context of strengthening the global response to the threat of climate change, sustainable development, and efforts to eradicate poverty[V. Masson-Delmotte, P. Zhai, H. O. Pörtner, D. Roberts, J. Skea, P.R.Shukla,A. Pirani, W. Moufouma-Okia, C.Péan, R. Pidcock, S. Connors, J. B. R. Matthews, Y. Chen, X. Zhou, M. I. Gomis, E. Lonnoy, T. Maycock, M. Tignor, T. Waterfield(eds.)].In Press.

James, R., Washington, R., 2013. Changes in African temperature and precipitation associated with degrees of global warming. Clim. Chang. 117(4), 859-872.

James, R., Washington, R. and Jones, R., 2015. Process-based assessment of an ensemble of climate projections for West Africa. J. Geophys. Res.: Atmos. 120(4), pp.1221-1238.

Jenkins, G.S., Gaye, A.T., Sylla, B., 2005. Late 20th century attribution of drying trends in the Sahel from the Regional Climate Model (RegCM3). Geophys. Res. Lett. 32(22).

Jones, C.G., Giorgi, F., Asrar, G., 2011. The Coordinated Regional Downscaling Experiment: CORDEX—An international downscaling link to CMIP5. *CLIVAR Exchanges,* No. 56, International CLIVAR Project Office, Southampton, United Kingdom, 34–39.

Kay, J.E., Deser, C., Phillips, A., Mai, A., Hannay, C., Strand, G., Arblaster, J.M., Bates, S.C., Danabasoglu, G., Edwards, J., Holland, M., 2015. The Community Earth System Model (CESM) large ensemble project: A community resource for studying climate change in the presence of internal climate variability. BAMS. 96(8), 1333-1349.

Kimura, F., Kitoh, A., 2007. Downscaling by pseudo global warming method. *The Final Report of ICCAP*, *4346*.

Klein, C., Heinzeller, D., Bliefernicht, J., Kunstmann, H., 2015. Variability of West African monsoon patterns generated by a WRF multi-physics ensemble. Clim. Dyn. 45(9–10), 2733–2755

Le Barbe, L., Lebel, T., Tapsoba, D., 2002. Rainfall variability in West Africa during the years 1950-90. J. Clim. 15, 87-202.

Lebel, T., Diedhiou, A., Laurent, H., 2003. Seasonal cycle and interannual variability of the Sahelian rainfall at hydrological scales. J. Geophys. Res., 108, 8389. doi: 10.1029/2001JD001580

Liu, C., Ikeda, K., Rasmussen, R., Barlage, M., Newman, A.J., Prein, A.F., Chen, F., Chen, L., Clark, M., Dai, A., Dudhia, J., 2017. Continental-scale convection-permitting modeling of the current and future climate of North America. Clim. Dyn. 49(1-2), 71-95.

Lupo, A., Kininmonth, W., Armstrong, J.S. and Green, K., 2013. Global climate models and their limitations. Climate change reconsidered II: Phys. Sci. 9, 148.

Marsham, J.H., Dixon, N.S., Garcia-Carreras, L., Lister, G.M., Parker, D.J., Knippertz, P. and Birch, C.E., 2013. The role of moist convection in the West African monsoon system: Insights from continental-scale convection-permitting simulations. Geophy. Res. Lett. 40(9), 1843-1849.

Martinkova, M., Kysely, J., 2020. Overview of Observed Clausius-Clapeyron Scaling of Extreme Precipitation in Midlatitudes. Atmos., 11(8), 786. https://doi.org/10.3390/atmos11080786

Martínez-Castro, D., Vichot-Llano, A., Bezanilla-Morlot, A., Centella- Artola, A., Campbell, J., Giorgi, F., Viloria-Holguin, C.C., 2017. The performance of RegCM4 over the Central America and Caribbean regions using different cumulus parameterizations. Clim. Dyn., 50, 4103–4126, https://doi.org/10.1007/s00382-017-3863-y.

Maynard, K., Royer, J.F., Chauvin, F., 2002. Impact of greenhouse warming on the West African summer monsoon. Clim. Dyn. 19(5-6), 499-514.

McMichael, A.J., Campbell-Lendrum, D.H., Corvalan, C.F., Ebi, K.L., Githeko, A.K., Scheraga, J.D., Woodward, A., 2003. Clim. Chang. Hum. Heal. 145-186. Geneva, World Health Organization.

Meinshausen, M., Smith, S.J., Calvin, K., Daniel, J.S., Kainuma, M.L.T., Lamarque, J.F., Matsumoto, K., Montzka, S.A., Raper, S.C.B., Riahi, K., Thomson, A.G.J.M.V., 2011. The RCP greenhouse gas concentrations and their extensions from 1765 to 2300. Clim. Chang. *109*(1-2), 213.

Monerie, P.A., Sanchez-Gomez, E. and Boé, J., 2017. On the range of future Sahel precipitation projections and the selection of a sub-sample of CMIP5 models for impact studies. Clim Dyn. 48(7-8), 2751-2770.

Monerie, P.A., Wainwright, C.M., Sidibe, M., Akinsanola, A.A., 2020. Model uncertainties in climate change impacts on Sahel precipitation in ensembles of CMIP5 and CMIP6 simulations. Clim. Dyn. 1-17. https://doi.org/10.1007/s00382-020-05332-0

Muhati, G.L., Olago, D. and Olaka, L., 2018. Past and projected rainfall and temperature trends in a sub-humid Montane Forest in Northern Kenya based on the CMIP5 model ensemble. Glob. Ecol. Conserv. 16, p.e00469. https://doi.org/10.1016/j.gecco.2018.e00469

NCEP FNL 2000. National Centers for Environmental Prediction/ National Weather Service/ NOAA/U.S. Department of Commerce (2000) updated daily. NCEP FNL Operational Model Global Tropospheric Analyses, continuing from July 1999. Research Data Archive at the National Center for Atmospheric Research, Computational and Information Systems Laboratory. https://doi. org/10.5065/D6M043C6. (accessed 9 March 2017)

Nicholson, S. E., 2013. The West African Sahel: A Review of Recent Studies on the Rainfall Regime and Its Interannual Variability. ISRN Meteorol. Article ID 453521, Vol. 2013 (32 pages). http://dx.doi.org/10.1155/2013/453521

Nikulin, G., Jones, C., Giorgi, F., Asrar, G., Büchner, M., Cerezo-Mota, R., Christensen, O.B., Déqué, M., Fernandez, J., Hänsler, A., van Meijgaard, E., 2012. Precipitation climatology in an ensemble of CORDEX-Africa regional climate simulations. J. Clim. 25(18), 6057-6078.

Noble E, Druyan LM, Fulakeza M, 2017. The sensitivity of WRF daily summertime simulations over West Africa to alternative parameter- izations. Part II: precipitation. Mon. Weather Rev. 145(1), 215–233

Oguntunde, P. G., Abiodun, B. J., Lischeid, G., 2011. Rainfall trends in Nigeria, 1901-2000. J. Hydrol. 411, 207-218. doi: 10.1016/j.jhydrol.2011.09.037

Omotosho, J. B., Abiodun, B.J., 2007. A numerical study of moisture build-up and rainfall over West Africa. Met. Apps. 14(3), 209-225. doi: 10.1002/met.11

Prein, A.F., Gobiet, A., Suklitsch, M., Truhetz, H., Awan, N.K., Keuler, K., Georgievski, G., 2013. Added value of convection permitting seasonal simulations. Clim. Dyn. 41(9-10), 2655-2677.

Attada, R., Parekh, A., Chowdary, J.S., Gnanaseelan, C., 2015. Assessment of the Indian summer monsoon in the WRF regional climate model. Clim. Dyn., 44, 3077–3100. https:// doi.org/10.1007/s00382-014-2295-1.

Attada, R., Dasari, H.P., Kunchala, R.K., Langodan, S., Niranjan Kumar, K., Knio, O., Hoteit, I., 2020. Evaluating Cumulus Parameterization Schemes for the Simulation of Arabian Peninsula Winter Rainfall. J. Hydrometeorol., 21(5), 1089-1114.

Rasmussen, R., Ikeda, K., Liu, C., Gochis, D., Clark, M., Dai, A., Gutmann, E., Dudhia, J., Chen, F., Barlage, M., Yates, D., 2014. Climate change impacts on the water balance of the Colorado headwaters: high-resolution regional climate model simulations. J. Hydromet. 15(3), 1091-1116.

Rasmussen, R., Liu, C., Ikeda, K., Gochis, D., Yates, D., Chen, F., Tewari, M., Barlage, M., Dudhia, J., Yu, W. and Miller, K., 2011. High-resolution coupled climate runoff simulations of seasonal snowfall over Colorado: a process study of current and warmer climate. J. Clim. 24(12), 3015-3048.

Riahi, K., Rao, S., Krey, V., Cho, C., Chirkov, V., Fischer, G., Kindermann, G., Nakicenovic, N., Rafaj, P., 2011. RCP 8.5—A scenario of comparatively high greenhouse gas emissions. Clim. Chang. 109(1-2), 33.

Roehrig, R., Bouniol, D., Guichard, F., Hourdin, F., Redelsperger, J.L., 2013. The present and future of the West African monsoon: A process-oriented assessment of CMIP5 simulations along the AMMA transect. J. Clim. 26(17), 6471-6505.

Sato, T., Kimura, F., Kitoh, A., 2007. Projection of global warming onto regional precipitation over Mongolia using a regional climate model. J. Hydro. 333(1), 144-154.

Schmidli, J., Frei, C., Vidale, P.L., 2006. Downscaling from GCM precipitation: a benchmark for dynamical and statistical downscaling methods. Int. J. Climatol. 26(5), 679-689.

Shongwe, M.E., Van Oldenborgh, G.J., Van Den Hurk, B.J.J.M., De Boer, B., Coelho, C.A.S., Van Aalst, M.K., 2009. Projected changes in mean and extreme precipitation in Africa under global warming. Part I: Southern Africa. J. Clim. 22(13), 3819-3837.

Shongwe, M.E., van Oldenborgh, G.J., van den Hurk, B., van Aalst, M., 2011. Projected changes in mean and extreme precipitation in Africa under global warming. Part II: East Africa. J. Clim. 24(14), 3718-3733.

Sultan, B., S. Janicot, 2000. Abrupt shift of the ITCZ over West Africa and intra-seasonal variability. Geophys. Res. Lett., 27, 3353-3356.

Sultan, B., Gaetani, M., 2016. Agriculture in West Africa in the twenty-first century: climate change and impacts scenarios, and potential for adaptation. Front. Plant Sci. 7, 1262.

Sylla, M.B., Diallo, I., Pal, J.S., 2013a. West African monsoon in state-of-the-science regional climate models. In *Climate Variability-Regional and Thematic Patterns*. IntechOpen.

Sylla MB, Giorgi F, Coppola E, Mariotti L, 2013b. Uncertainties in daily rainfall over Africa: assessment of gridded observation products and evaluation of a regional climate model simulation. Int. J. Climatol. 33(7), 1805–1817. https://doi.org/10.1002/joc.3551

Van Zomeren, J. and Van Delden, A., 2007. Vertically integrated moisture flux convergence as a predictor of thunderstorms. Atmosph Res, 83(2-4), 435-445. https://doi.org/10.1016/j.atmosres.2005.08.015

Wild, M., Ohmura, A., Gilgen, H., Roeckner, E., 1995. Regional climate simulation with a high resolution GCM: surface radiative fluxes. Clim. Dyn. 11(8), 469-486. https://doi.org/10.1007/BF00207196

De Xue, Y., Sales, F., Lau, K.M.W., Boone, A., Feng, J., Dirmeyer, P., Guo, Z., Kim, K.M., Kitoh, A., Kumar, V., Poccard-Leclercq, I., LC, 2010. Intercomparison and analyses of the climatology of the West AfricanMonsoon in the West African Monsoon modeling and evaluation project (WAMME) first model intercomparison experiment. Clim Dyn, 35, 3-27.

Xiang, H.W., 2005. The corresponding-states principle and its practice: thermodynamic, transport and surface properties of fluids. Elsevier.

List of Tables

List of Figures

Figure 12: Time-averaged vertical profiles of (a) air temperature (T), (b) specific humidity (q), and (c) zonal-component (u) of horizontal wind speed derived from ERA5, WRF current and PGW climate. The plotted values are averaged over latitudes 5-15^{O}N and longitudes 10^{O}W-10^{O}E for the period June to September during which the monsoon is fully developed.

Figure 13: Vertically integrated moisture flux convergence (VIMFC) derived from ERA5, WRF current and PGW climate and averaged for the period June to September. The moisture flux is vertically integrated from 1000hPa to 300hPa, where the atmosphere becomes dry. The last column shows the difference in VIMFC between the current and PGW climates.

Table 1: Model greenhouse gas concentration to reflect the mid-year value of 2071-2100 (IPCC 2000, 2007, 2014). The current GHG concentration level is the mean value for 1976-2005 (same as in Gbode et al, 2020).

Greenhouse gas	Current	Future (RCP8.5)

Carbon dioxide (CO_2)	379 ppmv	801 ppmv
Methane (CH_4)	1774 ppbv	3564 ppbv
Nitrous oxide (N_2O)	319 ppbv	414 ppbv
Chlorofluorocarbons-11 (CFC-11)	251 ppt	86 ppt
Chlorofluorocarbons-12 (CFC-12)	538 ppt	211 ppt

Table 2: Total rainfall amount (mm) from GPCP and TRMM, and current and PGW WRF model for each climatic zone from March to October. Values in bold represents wet years where the total rainfall amount is greater than those of the dry years.

		GPCP	**TRMM**	**BMJ**	**nTDK**	**nSAS**	**BMJ8.5**	**nTDK8.5**	**nSAS8.5**
Monsoon	**Year**	**Guinea Coast (4-8ºN)**							
Dry	2001	1291	1423	1069	1107	1326	1100	1119	1370
	2011	1154	1311	1109	1132	1385	1079	1052	1471
Wet	2008	**1422**	**1607**	**1137**	**1202**	**1436**	**1186**	**1204**	**1566**
	2010	**1367**	**1592**	**1174**	1076	1341	**1179**	1109	**1484**
Normal	2007	1428	1520	1206	1272	1433	1304	1263	1557
		Savannah (8-11ºN)							
Dry	2001	1156	1121	1254	1135	1367	1189	1212	1466
	2011	1050	1015	1224	1183	1325	1301	1142	1448
Wet	2008	**1330**	**1260**	**1360**	**1281**	**1405**	**1417**	**1310**	1460
	2010	**1277**	**1185**	**1336**	**1251**	**1461**	**1438**	**1399**	**1521**
Normal	2007	1287	1212	1340	1217	1357	1363	1232	1428
		Sahel (11-15ºN)							
Dry	2001	672	603	652	461	723	782	490	758
	2011	588	558	621	450	616	727	420	684
Wet	2008	**765**	**708**	**703**	**596**	671	**789**	**590**	**779**
	2010	**774**	**730**	**752**	**605**	**791**	**860**	**583**	**830**
Normal	2007	719	624	692	557	742	810	541	810

Table 3: Fraction of convective and non-convective rainfall produced from the model runs. The domains considered are West Africa (0-20ºN and 20ºW-20ºE), Guinea Coast (4-8ºN and 10ºW-10ºE), Savannah (8-11ºN and 10ºW-10ºE) and Sahel (11-16ºN and 10ºW-10ºE).

Domain	**GD-MYJ-BMJ**	**WSM5-MYNN-nTDK**	**WSM5-YSU-nSAS**

	Convective	Non-convective	Convective	Non-convective	Convective	Non-convective
West Africa	0.64	0.36	0.96	0.04	0.93	0.07
Guinea Coast	0.75	0.25	0.98	0.02	0.96	0.04
Savannah	0.54	0.46	0.95	0.05	0.93	0.07
Sahel	0.57	0.43	0.94	0.06	0.85	0.15
	GD-MYJ-BMJ8.5		**WSM5-MYNN-nTDK8.5**		**WSM5-YSU-nSAS8.5**	
West Africa	0.61	0.39	0.95	0.05	0.93	0.07
Guinea Coast	0.72	0.28	0.97	0.03	0.96	0.04
Savannah	0.53	0.47	0.93	0.07	0.93	0.07
Sahel	0.56	0.44	0.88	0.12	0.83	0.17

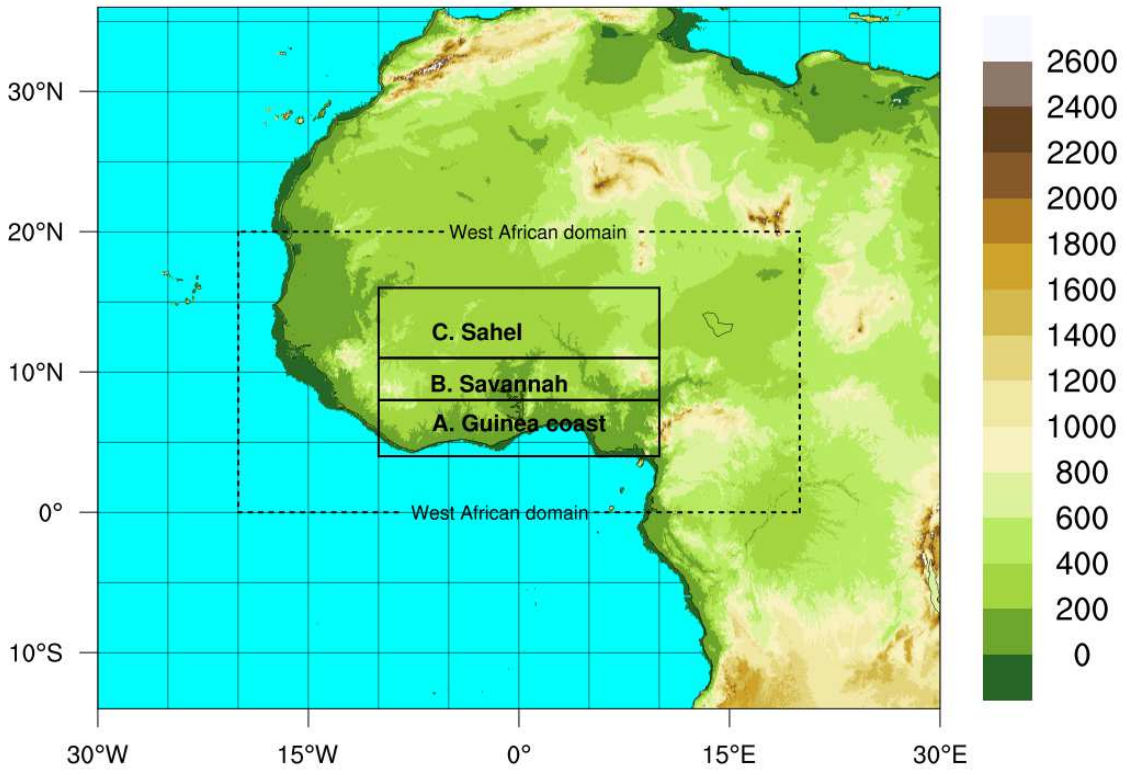

Figure 1: WRF model domain showing elevation in meters and highlights of the West African (0°–20° N, 20° W–20° E) region and the three climatic zones; A. Guinea coast (4-8ºN), B. Savannah (8-11ºN) and C. Sahel (11-16ºN) (Source: Gbode et al. 2019b)

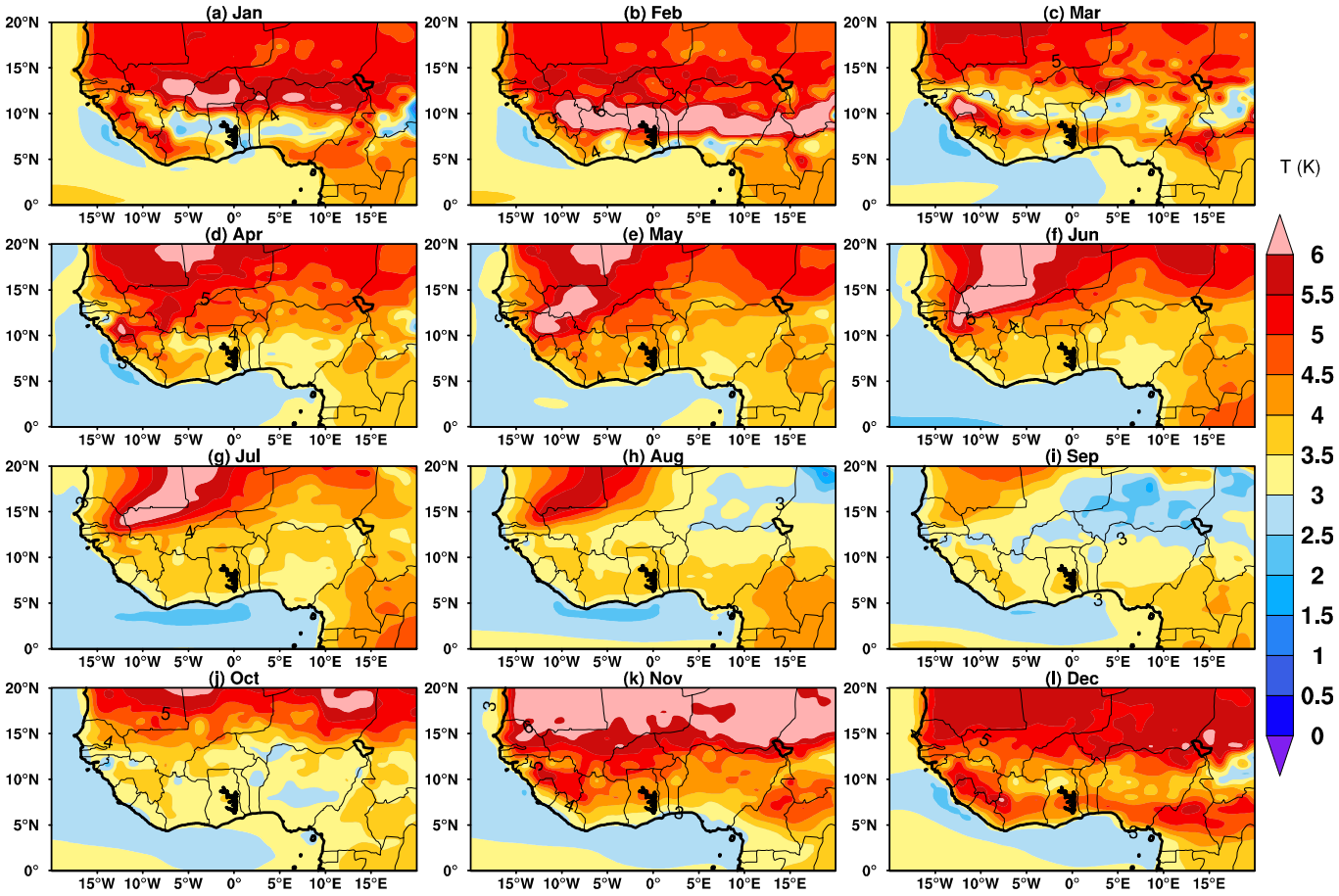

current (1976-2005) and future (2071-2100) climate. The LENS CESMv1-CAMv5.2 40-member ensemble of historical and RCP8.5 was used to produce the climate perturbation.

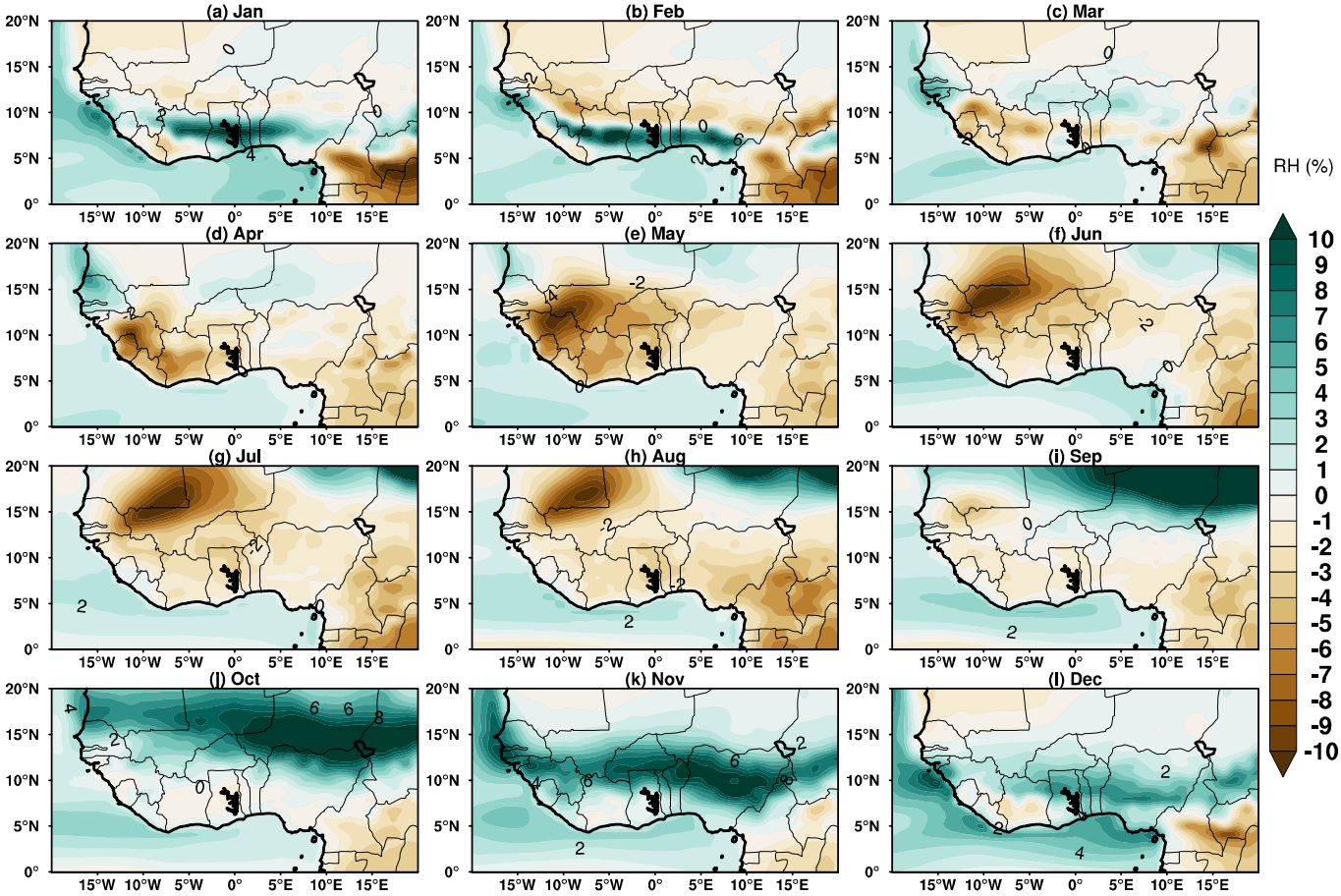

Figure 3: Same as Figure 2 but for near surface relative humidity.

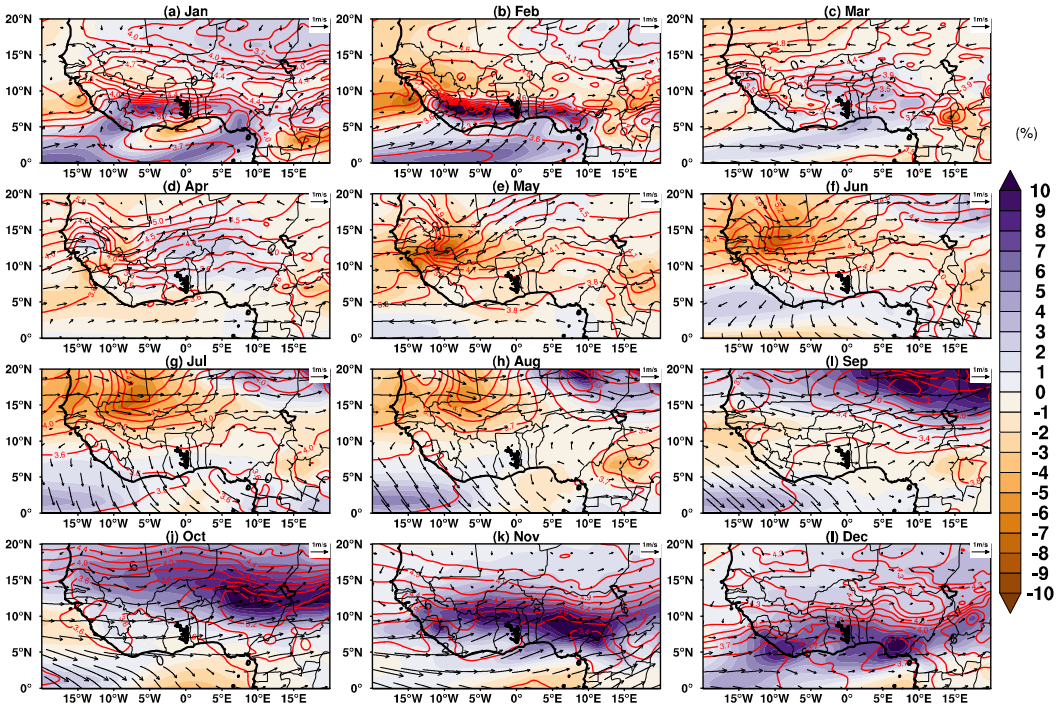

Fig at 850mb. The changes are derived from the difference between the current (1976-2005) and future (2071-2100) climates. The filled and red contours represent relative humidity and temperature, respectively. Wind vector of 1ms^{-1} is used as the reference wind difference.

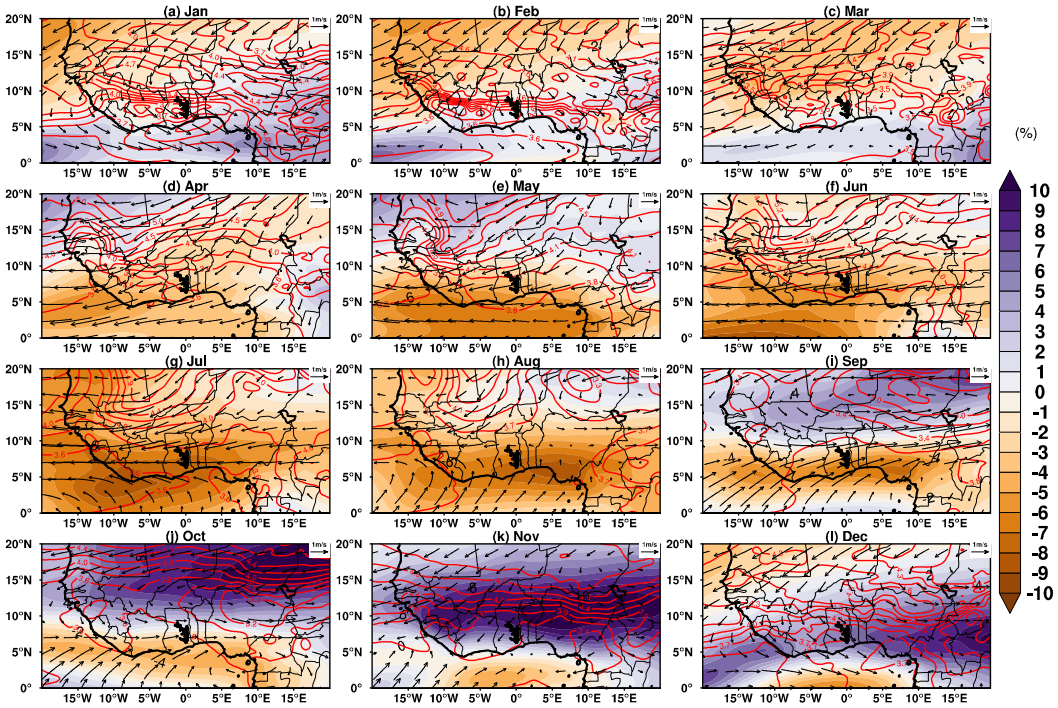
(a) Jan
(b) Feb
(c) Mar
(d) Apr
(e) May
(f) Jun
(g) Jul
(h) Aug
(i) Sep
(j) Oct
(k) Nov
(l) Dec
20°N
15°N
10°N
5°N
0°
15°W 10°W 5°W 0° 5°E 10°E 15°E
1m/s
(%)
10
9
8
7
6
5
4
3
2
1
0
-1
-2
-3
-4
-5
-6
-7
-8
-9
-10

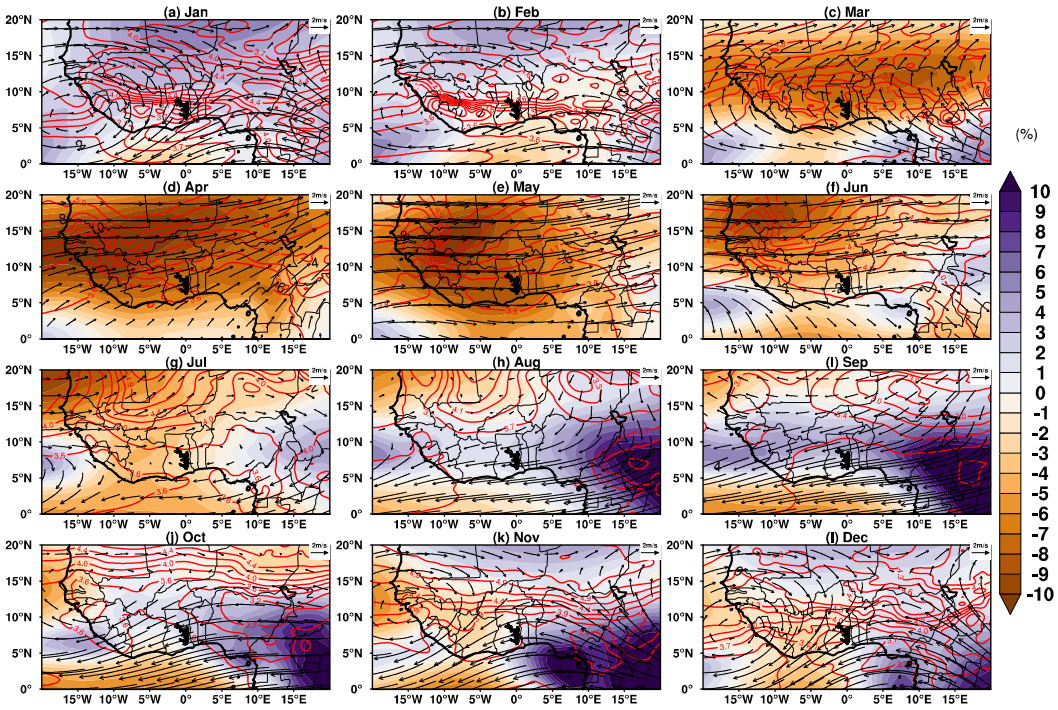

Figure 6: Same as Figure 4 but for 150mb pressure level.

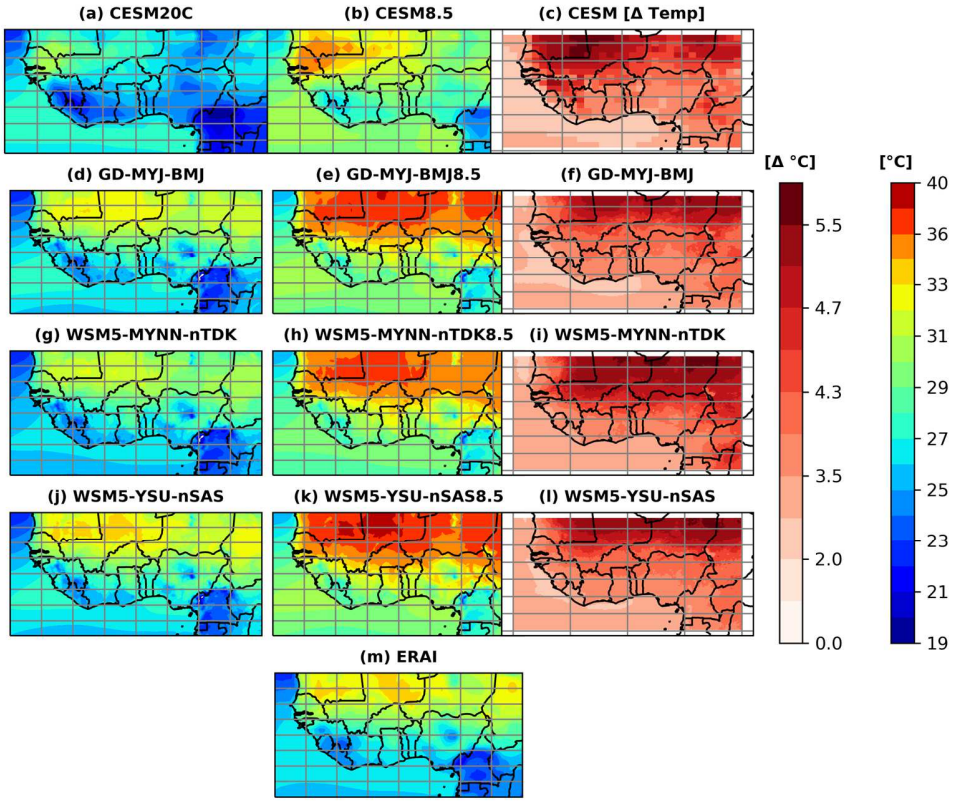

Figure 7: Distribution of surface air temperature averaged during the period March - October for ERAI reanalysis and model outputs (i.e. present and future runs). Panels a, d, g and j shows the current (20th Century) CEMS20C and WRF runs. For the future (2071-2100) CESM8.5 and the PGW runs are represented on panels b, e, h and k. The difference between PGW and present climate are depicted on the last column (c, f, i and l) while m is for ERAI. Values in the WRF model plots are averages derived from the selected five years (i.e. 2001, 2007, 2008, 2010 and 2011).

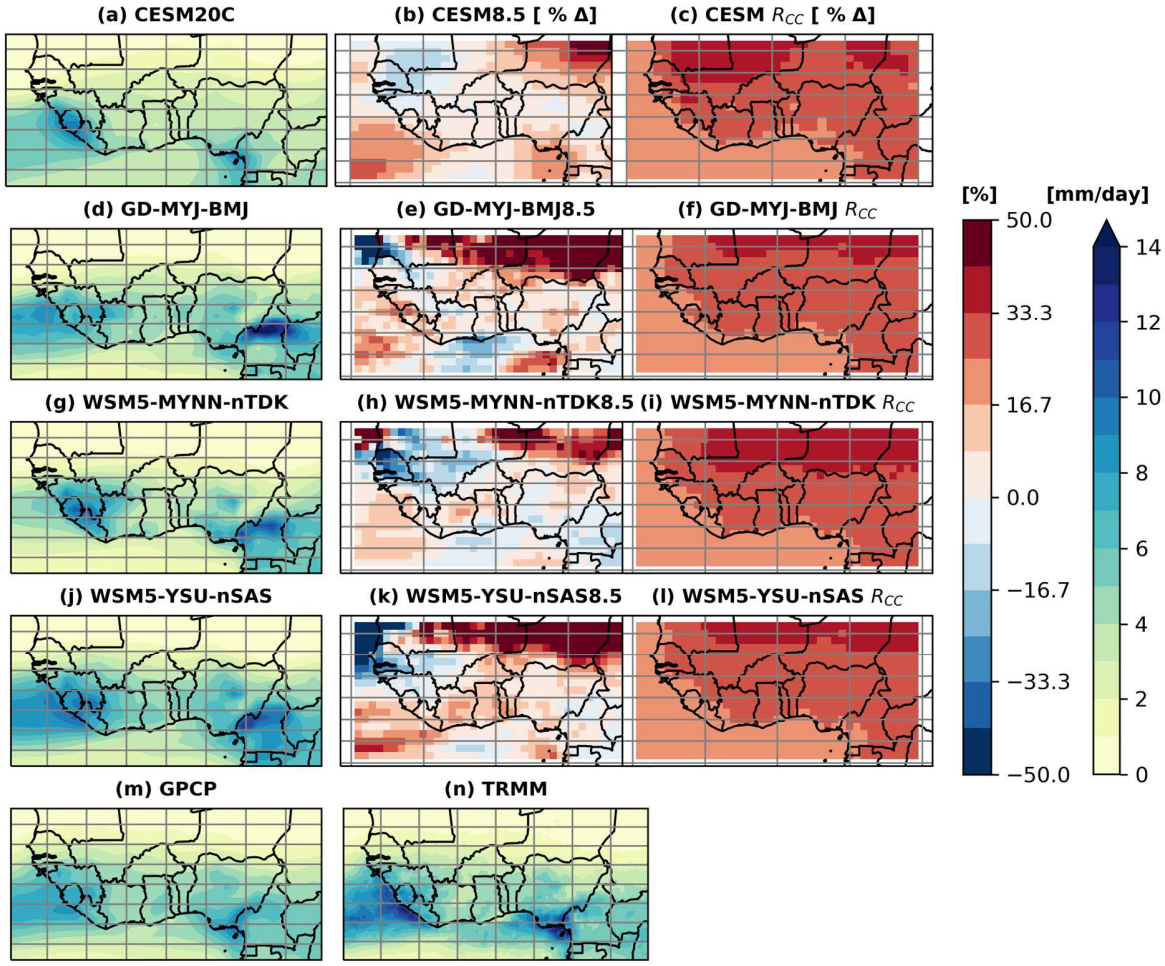

Figure 8: Spatial distribution of average daily rainfall amount (mm day^{-1}). Values of (a) CESM are averages derived from the considered 30years current climate, (b) shows the percentage change between future and current climate periods, (c) depicts the percentage change in rainfall derived from the Clausius-Clapeyron relation (R_{CC}), (d, g, and j) are WRF runs derived from the average of the five simulated years for the period March to October while the (e, h, and k) depicts the rainfall percentage difference between the PGW and current climates, (f, I and l) the rainfall percentage difference based on the R_{CC} relation, (m) GPCP and (n) TRMM.

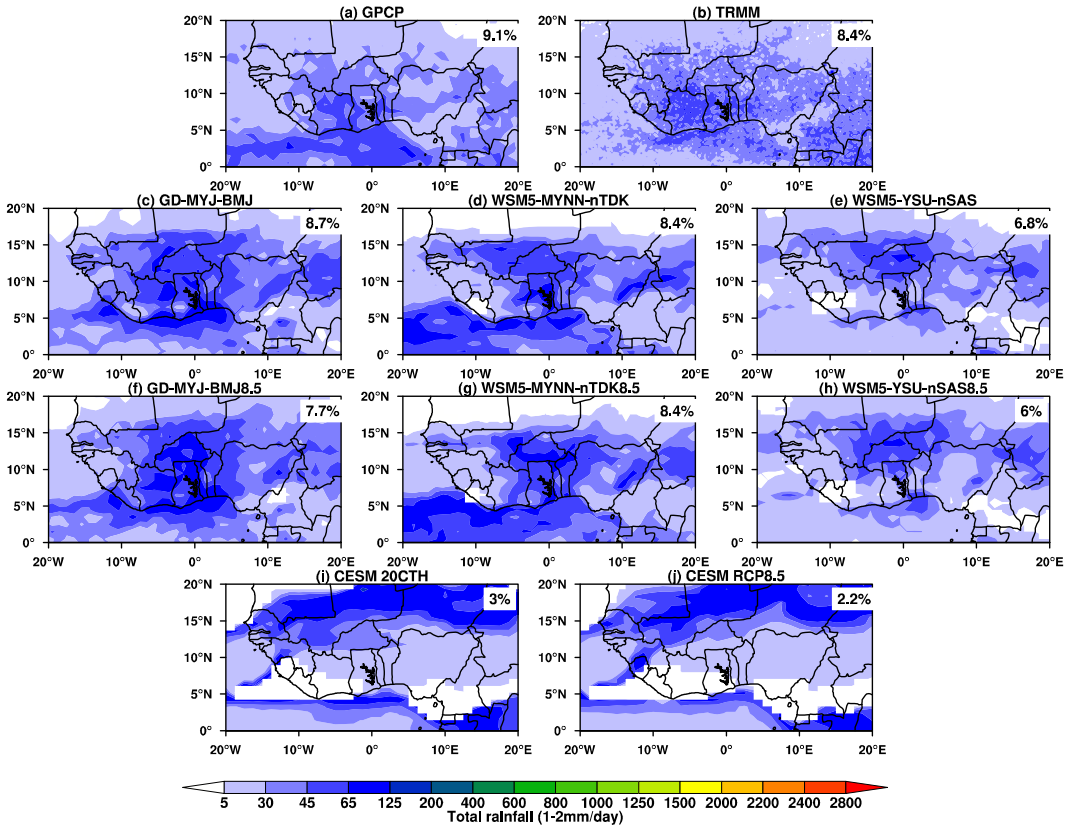

Figure 9: Total rainfall and percentage contribution from light rainfall (1-2mm) intensity received for the period March-October. GPCP, TRMM and WRF outputs are derived from the average of the selected five years while CESM20C and CESM85 are derived for the period 1976-2005 and 2071-2100, respectively.

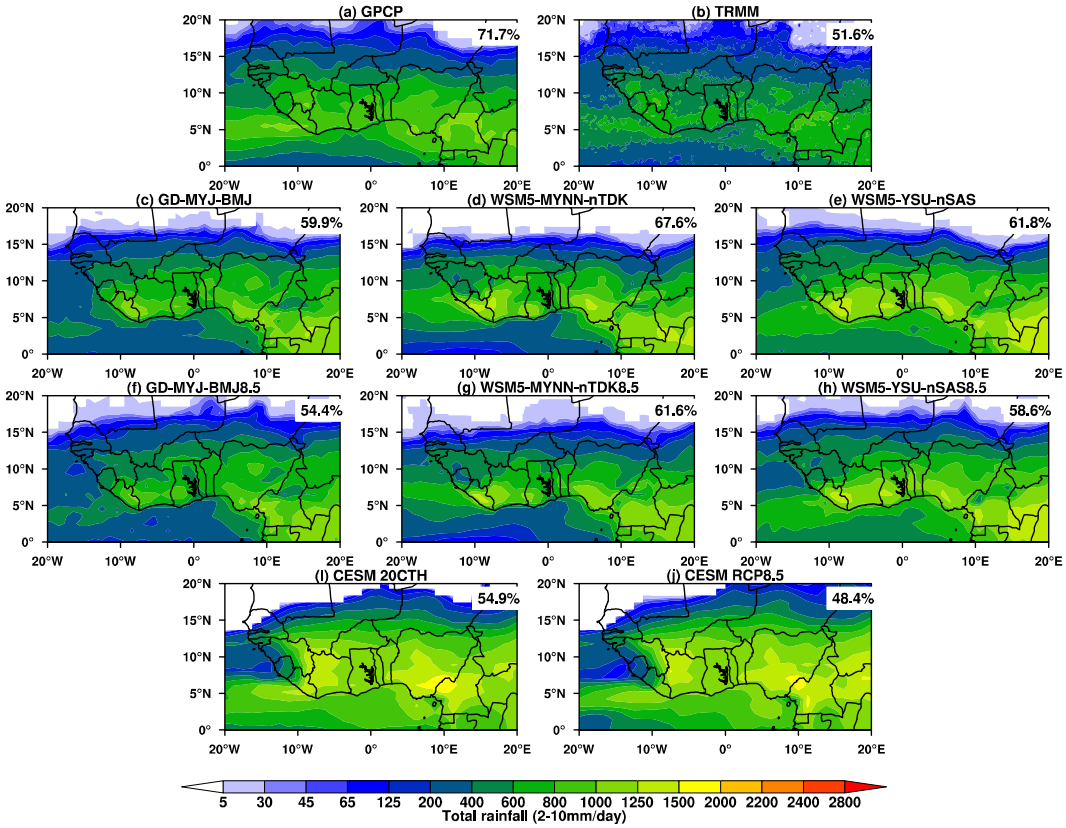

Figure 10: Same as Figure 9 but for moderate rainfall (>2-10mm) intensity.

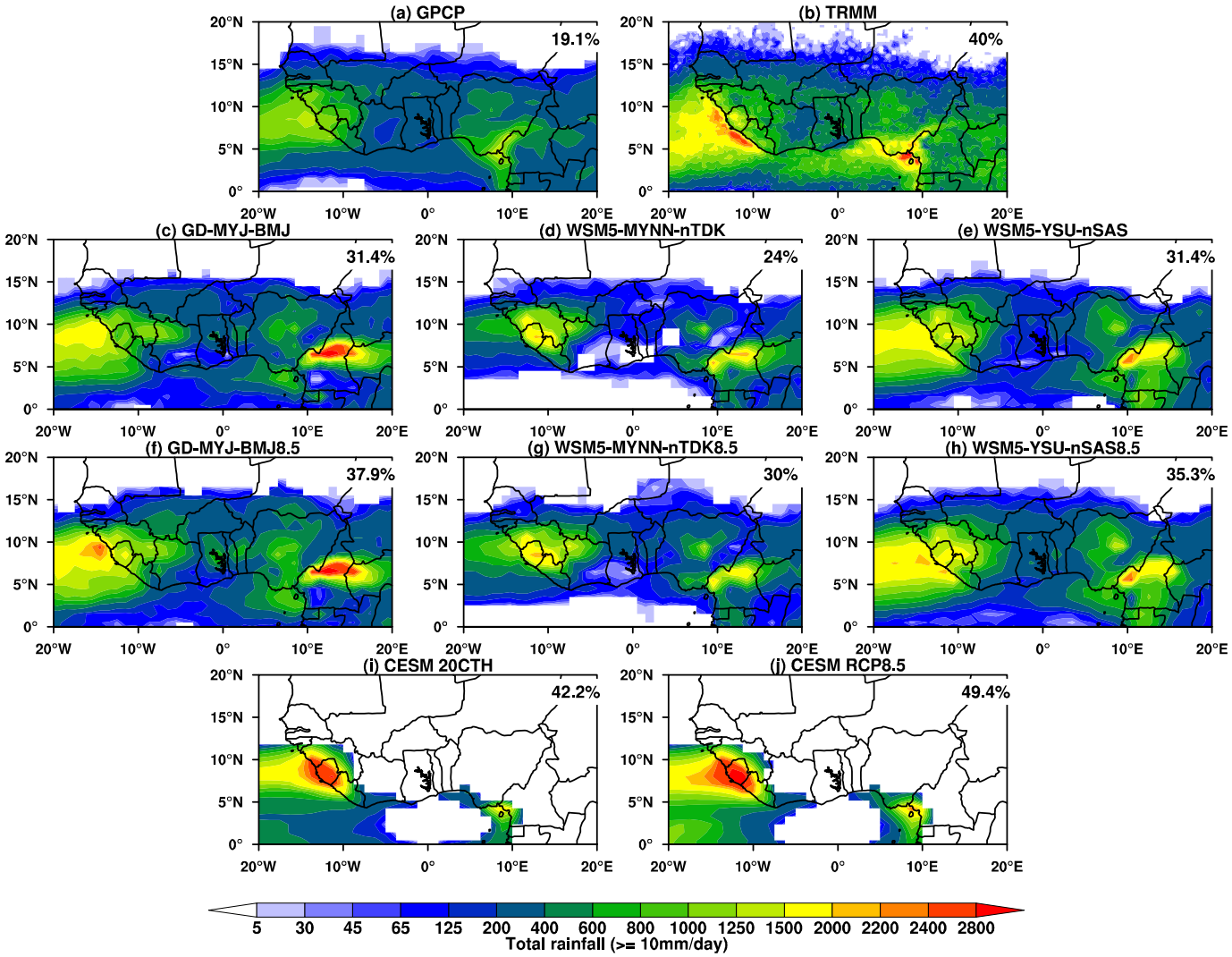

Figure 11: Same as Figure 9 but for heavy rainfall (10mm and above) intensity.

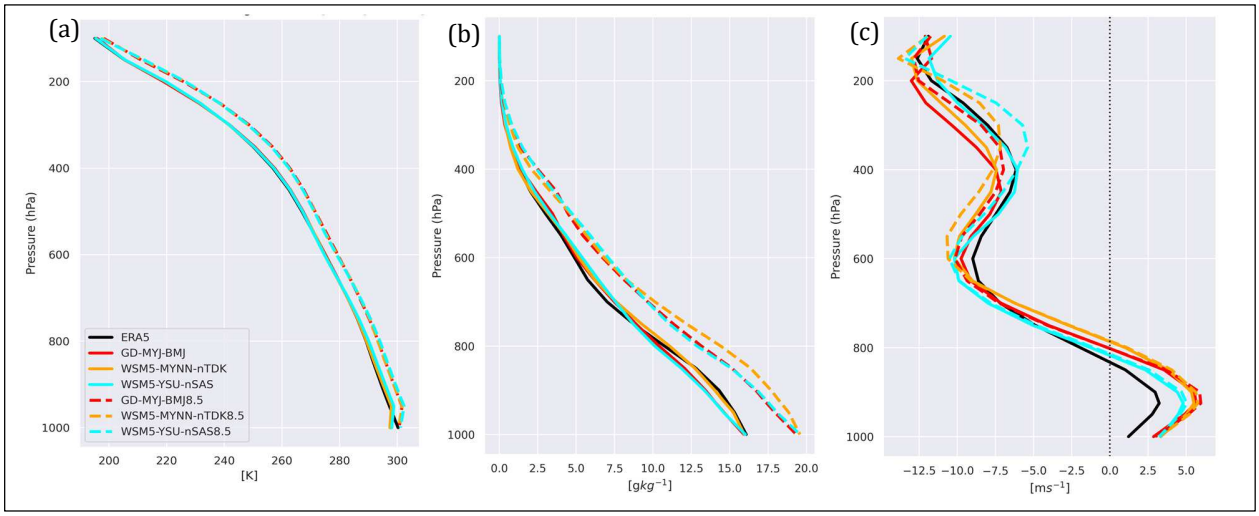

Figure 12: Time-averaged vertical profiles of (a) air temperature (T), (b) specific humidity (q), and (c) zonal-component (u) of horizontal wind speed derived from ERA5, WRF current and PGW climate. The plotted values are averaged over latitudes 5-15^{O}N and longitudes 10^{O}W-10^{O}E for the period June to September during which the monsoon is fully developed.

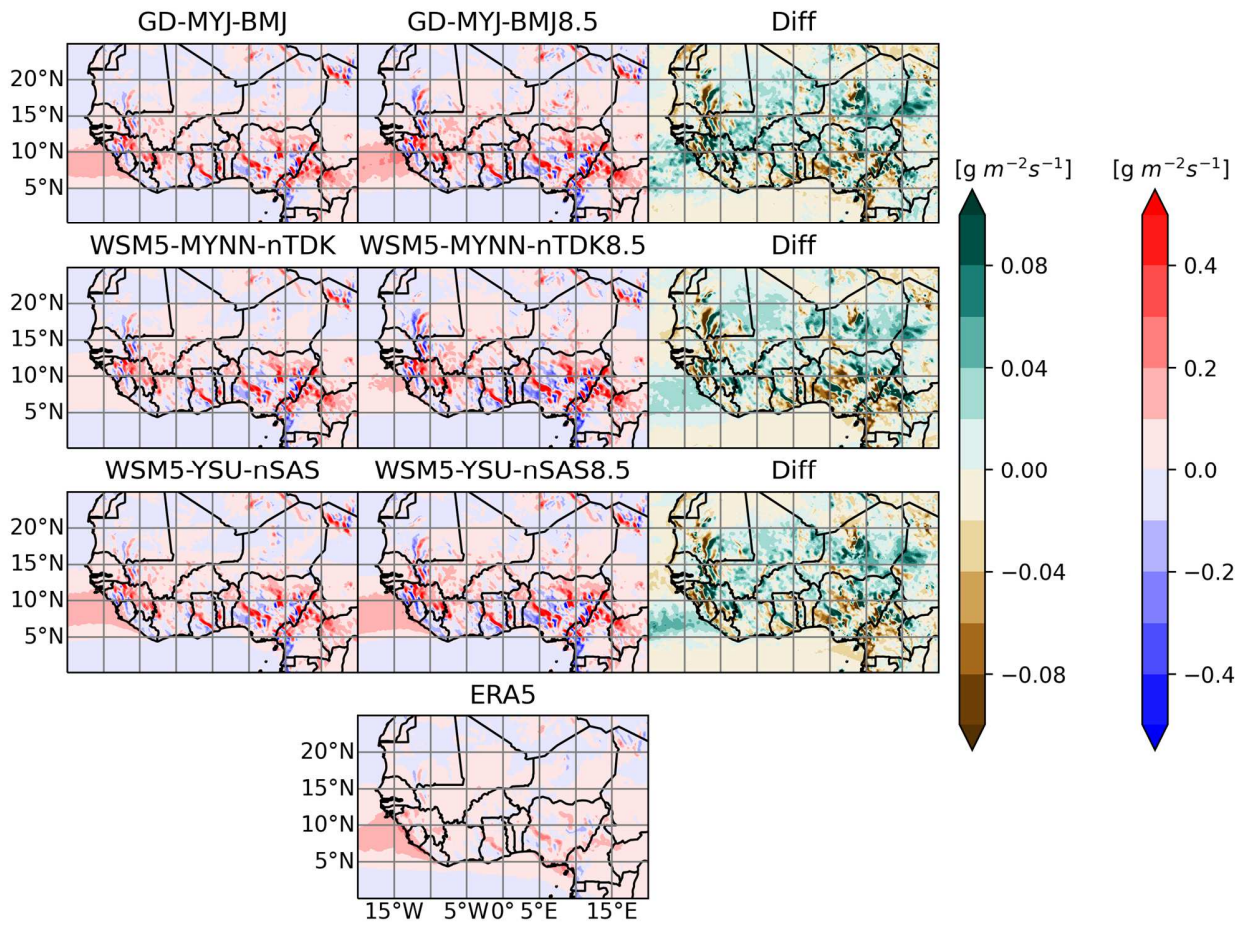

Figure 13: Vertically integrated moisture flux convergence (VIMFC) derived from ERA5, WRF current and PGW climate and averaged for the period June to September. The moisture flux is vertically integrated from 1000hPa to 300hPa, where the atmosphere becomes dry. The last column shows the difference in VIMFC between the current and PGW climates.